FACULTY OF SCIENCE
UNIVERSITY OF COPENHAGEN
NIELS BOHR INSTITUTE

Master's thesis

Jesper Sjolte

Interpretation of the Isotopic Composition of the Greenland Ice Cores Using Simple Modeling

Second Edition

Academic advisor: Sigfús J. Johnsen

First edition (submitted): 26/10/05

Second edition: 22/11/05

Abstract

A simple Rayleigh-type distillation model is used to simulate the isotopic composition of precipitation in Greenland. The present day isotopic composition of precipitation is simulated, and the relationship between depletion of heavy isotopes and temperature is investigated. This results in confirmation of two important observations from ealier studies: The $\delta^{18}O$ value is linearly related to the temperature in the cloud at the moment of deposition, and the deuterium excess is strongly correlated with the temperature of evaporation at the origin of the precipitation.

Using the model, selected climate shifts in the past 100.000 years are evaluated in terms of temperature. Both the Greenland site temperature and the moisture source temperature are considered, using ice core data from central Greenland. The results show temperature shifts of the correct magniture, though it appears that the shifts are slightly underestimated compared to results achieved by other methods.

Furthermore, the possibility of an additional Pacific moisture source during the last glacial is discussed. Moisture from the Pacific could have been transported north of the Laurentide Ice Sheet by a split jet stream during the winter. Such an additional main moisture source would demand a re-evaluation of the interpretation of the Greenland ice cores.

Preface to the Second Edition

This is the second edition of my master's thesis originally submitted the 26th of October 2005. The reason for this revised version, is the correction of a few errors found in the original report. The most important corrections have been made in Figure 4.7 and Table 5.1.

Department of Geophysics, University of Copenhagen Jesper Sjolte

November 2005

Preface to the First Edition

Since the discovery in the fifties of the connection between temperature and the isotopic composition of precipitation, the discipline of extracting past temperature variations from ice core data, has developed into an independent field within the subject of isotope glaciology. This involves both extensive field work, extracting deep ice cores from ice sheets, doing the isotope measurements, and modeling using both simple isotope models and complex atmospheric circulation models with isotopic tracers.
The Greenland ice cores contain climate information dating as far back as the previous interglacial, the Eemian. Climate shifts appear as changes in the isotopic composition of the ice. By understanding the physics, which govern isotopic composition of the ice, one can estimate the magnitude of climate changes in terms of temperature. The knowledge of the magnitude of past climate changes is important for understanding the nature of natural climate variations. We would like to answer the question: *What climate changes is nature capable of?*

The goal of this study is to calculate the temperature changes in Greenland and the temperature changes in the main moisture source for Greenland precipitation, during climate shifts in the past 100.000 years, using a simple isotope model.
The isotope model used by Johnsen et al. [35] has been modified as a part of this study. The modified model is used to investigate the relationship between the isotopic composition of precipitation and the temperatures at the Greenland site and at the main moisture source. By knowing the past and present isotopic composition of the precipitation in Greenland from ice cores, the drill site and moisture source temperature can be calculated.

Structure and Notation

Chapter 1 of this thesis is a general introduction to the connection between climate variations and the isotopic components of water.
Chapter 2 and **3** give a description of the physics needed to construct a

simple isotope model. Chapter 2 describes the meteorology involved, while Chapter 3 deals with the isotopic changes of water during phase transition.
In **Chapter 4** the isotope model is presented, and the performances of the original and modified version are compared. The use of simple models to simulate the isotopic composition of precipitation will also be discussed in this chapter.
The estimated temperature amplitudes of selected climate shifts are given in **Chapter 5**. This chapter also includes a comparison with work done by others, and a presentation of recent results impacting the interpretation of ice cores.
In **Chapter 6** the important points are summarized, and a scope of possible future investigations is given.
After Chapter 6 additional material is given in the **Appendix**, and references are listed in the **Bibliography**. References are given with numbers in square brackets.
It should be noted that ages sometimes are followed by **yr BP** or **kyr BP**, meaning years before present or thousand years before present, respectively. In this context the present is 1950.
Temperatures are always in °C.

Ackowledgements

I would like to thank the following people: Tais W. Dahl for helping me improve this thesis, and for reminding me of the constant possiblity of doing better, Marie-Louise Siggaard-Andersen for introducing me to the applications of glaciochemical analysis, and Susanne Lilja Buchard for correcting many errors and improving the overall readability during the finishing stages of the work on this thesis. I would also like to thank my family for support during my years of studying.
Last but not least, thank should be given to my advisor Sigfus J. Johnsen for exellent and always inspiring counseling.

Department of Geophysics, University of Copenhagen Jesper Sjolte

October 2005

Contents

Chapter 1

Isotopes and Climate

This chapter is an introduction to the relationship between Earth's climate and the isotopic components of water. This includes a brief presentation of isotope data and the glacial climate.

1.1 The Isotopic Components of Water

The three main isotopic components of water are $H_2^{16}O$, $HD^{16}O$, and $H_2^{18}O$, where $H_2^{16}O$ is the most abundant. The isotopic composition of a sample of, for example, collected precipitation or glacier ice is usually expressed with the δ relationship defined by Craig [12]

$$\delta = \frac{R - R_{SMOW}}{R_{SMOW}} \cdot 1000‰ \tag{1.1}$$

where R can be the isotopic ratios of either [D]/[H] or $[^{18}O]/[^{16}O]$, and R_{SMOW} is the defined standard for isotopic ratios for water abbriviated SMOW (Standart Mean Ocean Water). Using the δ relationship defined in equation (1.1), one expresses to which degree a sample is depleted with respect to the heavy isotopes relative to SMOW.

1.1.1 The Isotopic Composition of Precipitation

The depletion of a water sample depends on the history and origin of the water. As a general rule the δ value of precipitation decreases when going towards the poles. This pole ward depletion exists because of succesive isotopic fractionation during condensation, as the heavy isotopes condense more

readily than the lighter ones. As opposed to the fresh water of precipitation and lakes, sea water is generally uniform[1] in isotopic composition (Epstein & Mateda [19]).
The first to relate isotopic composition of precipitation to temperature was W. Dansgaard [16]. Dansgaard later established an empirical relationship between the annual mean $\delta^{18}O$ and the annual mean temperature of the surface air based on Greenland inland and coastal measurements (Dansgaard [15]):

$$\delta^{18}O = 0.69T - 13.6‰ \tag{1.2}$$

This simple empirical relation was found to be robust for the Greenland area, and expresses the spatial slope of $\delta^{18}O$ versus temperature. A similar relationship holds for deuterium.
A linear relation similar to equation (1.2) was found by Johnsen et al. [35] based on newer data from South and West Greenland stations:

$$\delta^{18}O = (0.67 \pm 0.02)T - (13.7 \pm 0.5)‰ \tag{1.3}$$

This means that the spatial slope of $\delta^{18}O$ versus temperature is $0.67‰/°C$. The temporal variations of $\delta^{18}O$ versus temperature shows a different slope than equation (1.3). Shuman et al. [59] found a temporal slope of $0.46‰/°C$ for the $\delta^{18}O$ versus temperature relationship at Greenland Summit. This result shows that spatial and temporal slopes of $\delta^{18}O$ with temperature are different, and should not be interpreted as being consequences of the same mechanisms.
As mentioned above the isotopic ratio of water varies both geographically and temporally, due to fractionation processes under phase transitions of water (details are given in chapter 3). Traditionally the change in isotopic ratio is explained by a number of effects, which are discussed below.

Geographical Effects

Depletion of heavy isotopes in precipitation is connected to the distance the moisture is transported from the source of evaporation. Precipitation is observed to be increasingly depleted as the condensation progresses. This has three effects:

[1] Except for areas with large influx of fresh water from rivers or precipitation.

- When an air parcel is transported inland from the sea the precipitation will be progressively depleted, hence the continental effect.

- The second effect, the latitude effect is caused by transport of moist air from warm to cold regions. When transporting an air parcel towards colder high latitude regions the isotopic ratio will drop.

- The final geographic effect is caused by topography when an air parcel is forced to a higher elevation. Because of the lapse rate of the troposphere the temperature drops with altitude, reducing the moisture contents by condensation. This will cause elevated sites such as mountain tops and central parts of ice sheets to be depleted.

These geographical effects are illustrated in Figure 1.1.

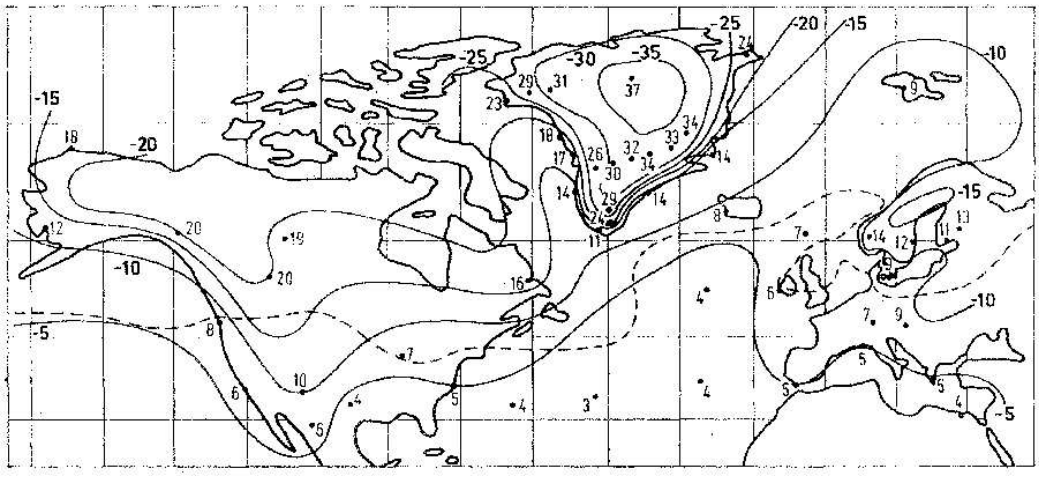

Figure 1.1: Numerical mean $\delta^{18}O$ values of annual precipitation and approximate δ-isolines (adapted from Dansgaard & Tauber [17]). All of the $\delta^{18}O$ values are in fact negative, so all positive values are printing errors. Note the low $\delta^{18}O$ values found in central Greenland.

Temporal Effects

There are two distinct temporal variations: The short term annual cycle and long term climatic variations. The temperature at a site will vary during the

year causing a seasonal isotopic change. Because the temperature amplitude increases with latitude, this effect will be greatest at high latitudes.
On longer time scales climate changes will affect the isotopic composition of precipitation. Climatic temperature changes are greatest at high latitudes also causing the largest amplitude in δ values. Induced circulation changes may also affect the δ if the path and origin of moisture is changed.
During a glaciation there will also be the possibility of an additional continental effect because of extended sea ice.
The distribution of precipitation during the annual cycle can also change with the climate. Werner et al. [65] has suggested that there was no winter precipitation at the Greenland Summit during the Last Glacial Maximum (LGM). Absence of winter precipitation would give a higher mean isotopic ratio, compared to the present situation where precipitation is accumulated approximately uniformly during the year (Shuman et al. [59]). This will be discussed further in Chapter 5.

1.1.2 The Deuterium Excess

Additional information from the precipitation can be drawn when measuring both $\delta^{18}O$ and δD. Craig [12] found a simple relation obeyed by $\delta^{18}O$ and δD in a large number of samples (see Figure 1.2).
The line $\delta D = 8\delta^{18}O + 10$ in Figure 1.2 is refered to as the Global Meteoric Water Line (GMWL). This relation was later redefined by Dansgaard [15] as the deuterium excess

$$d = \delta D - 8\delta^{18}O \tag{1.4}$$

Dansgaard interpretated d as a measure of non-equilibrium fractionation processes[2] during evaporation. This interpretation means that d gives us information of the evaporative conditions at the origin of the precipitation, which ultimately tells us about the history of the air parcel delivering the precipitation.

[2]Details are given in Section 3.2.

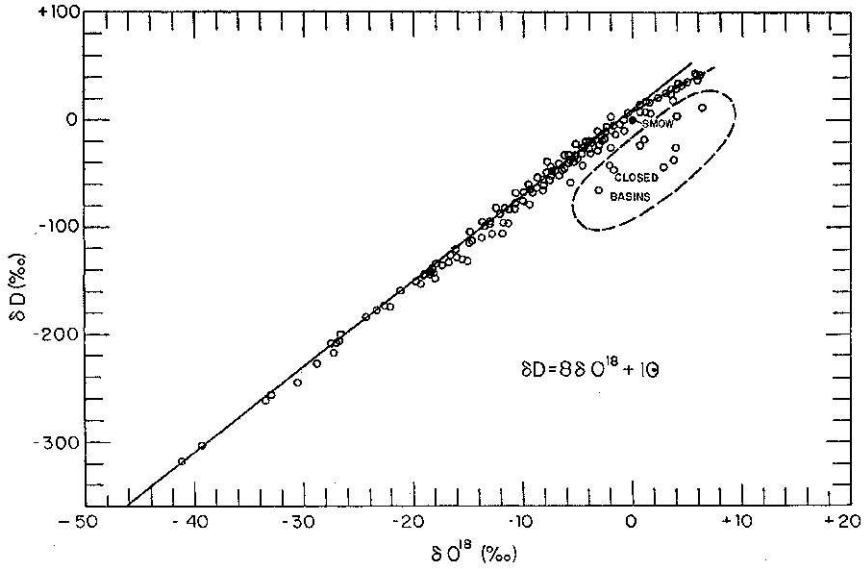

Figure 1.2: The δ variation for deuterium and oxygen-18 in rivers, lakes, rain and snow (adapted from Craig [12]).

1.2 Ice Cores

The polar ice sheets on Earth are masses of precipitation accumulated during thousands of years. With the link between temperature and δ values for precipitation the possibility of a palaeothermometer becomes evident.
Ice is a quasiviscous material, and will deform when exerted to pressure. This will cause large masses of ice to flow under the influence of gravity. The general flow lines of an ice sheet are shown in Figure 1.3. At the center of the ice sheet the flow lines diverge. This is denoted the ice divide. At the ice divide the flow is particularly simple, as the ice originates from the same point on the surface of the ice sheet. The flow here is restricted to a thinning of the annual layers as the ice moves towards the bottom. Consequently, the annual layers will be perfectly stratified, going back in time, moving from the top to the bottom.
This simple view of the flow in an ice sheet can be complicated by a number of things. On time scales of thousands of years the mass balance of the ice sheet might be disturbed by changes in the accumulation or ablation. This can change the height of the ice sheet or the location of the ice divide.
In areas with large geothermal heat flux the ice can reach the melting point at the bottom and cause melting of the oldest layers. Bottom topography also affects the ice flow and may cause folding of the stratification.

To obtain stratified records of the past precipitation ice cores have been drilled in Greenland and Antarctica. The ice cores have subsequently been analyzed to obtain δ values for ice thousands of years old. Drill sites are often located near an ice divide to ensure the best possible stratification.

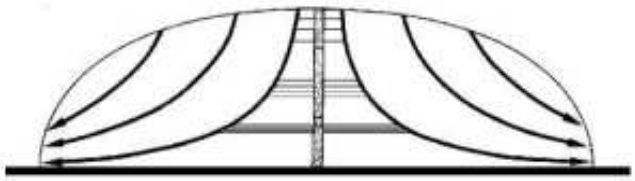

Figure 1.3: Schematic view of the flow in an ice sheet, with the thinning of the annual layers shown.

1.2.1 Introduction to Interpretation of Ice Cores

The age of a section of an ice core can be achieved by counting the annual cycles of the $\delta^{18}O$ signal. However, this method can only be used for dating the youngest $10 - 20$ thousand years, because of diffusion and thinning obliviating the high frequency part of the signal (Johnsen [30]).
The range of the counting method varies from site to site depending on the accumulation rate and other parameters affecting the ice flow. However, the range and accuracy of the counting method can be improved by also considering the annual variation of the chemical composition of the ice together with the $\delta^{18}O$ signal (Rasmussen et al. [54]). In older parts of the core the age is estimated with great succes by flow models (Johnsen & Dansgaard [31], Johnsen et al. [33]).
The isotope signal from two deep ice cores is shown in Figure 1.4. An important feature is the transition from the last glacial to our present interglacial, the Holocene, dated 11738 yr BP (Rasmussen et al. [53]). The transition is recognized as a large shift in δ values. In the case of GRIP and NGRIP this shift is approximately $7‰$.
The two cores presented here show very similar variations in $\delta^{18}O$ during the past 110.000 years, with major features being recognizable in both cores. NGRIP does however tend to have lower glacial values. The last glacial reached it's maximum 21.000 years ago, which is refered to as LGM. This is defined as the maximum extent of the ice sheets, which does not coincide with the most negative $\delta^{18}O$ values in the ice cores. The $\delta^{18}O$ values are

low during LGM, but more negative values are found in earlier parts of the glaciation.

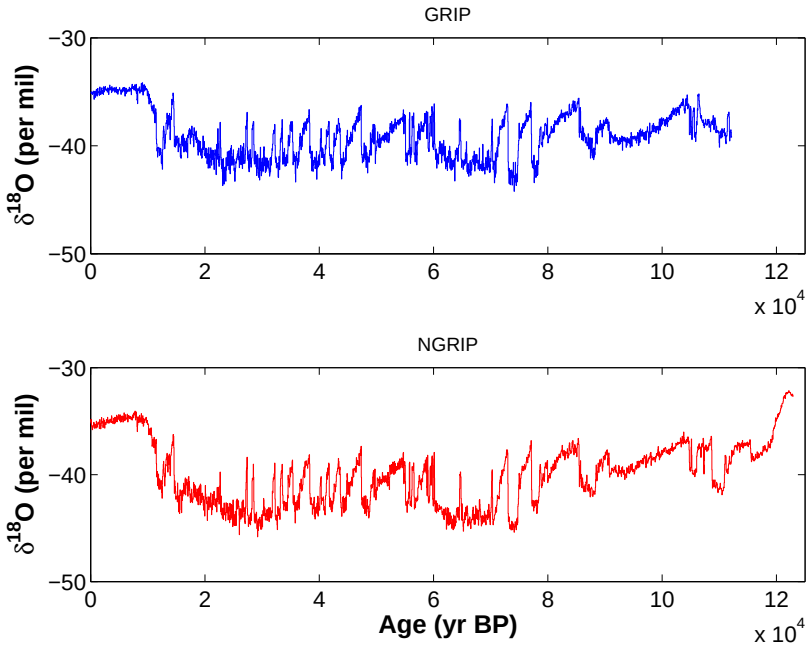

Figure 1.4: The $\delta^{18}O$ values of the GRIP (top) and NGRIP (bottom) ice cores dating back to the previous interglacial (data is from Johnsen et al. [32] and NorthGRIP Members [49]). The GRIP and NGRIP sites are located in central Greenland, NGRIP being about 300km north-northwest of GRIP.

The bottom part of the GRIP core is not shown, as the flow in this part has been disturbed by bottom topography (Fuchs & Leuenberger [21]). The oldest part of the NGRIP core show high δ values, which are in fact less negative than present δ values, suggesting warmer temperatures. This part of the core is ice from the previous interglacial, the Eemian.
During the glacial many variations occur on time scales of hundreds of years. The variations have an amplitude of approximately 5‰, and have a saw tooth shape, with a sharp rise in $\delta^{18}O$ followed by a slow drop off. This is not observed during the Holocene. These fast variations are the Dansgaard-Oeschger oscillations (D/O) (Dansgaard et al. [18]). The cause of D/O is belived to be ice sheet dynamics coupled with reorganization of ocean currents, causing an increased flux of ice bergs to the ocean associated with the collapse of ice sheets. Ice bergs bring continental material with them as the

are transported to the ocean. This can be seen as Ice Rafted Debris (IRD) in marine cores. For the most severe D/O the marine cores show an increase in the flux and a change in composition of IRD, compared to less severe D/O (Bond et al. [4]). This is known as Heinrich events. The warm periods (high δ) during D/O are denoted interstadials and the cold periods (low δ) are stadials.

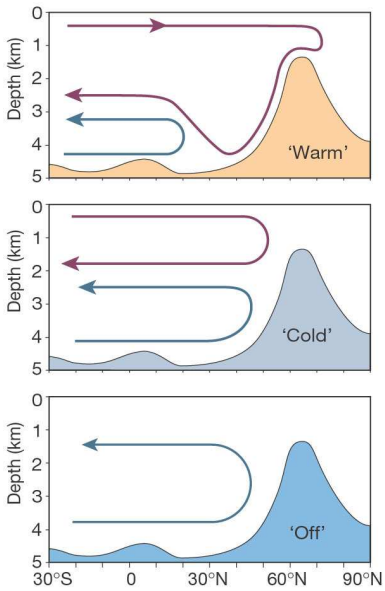

Figure 1.5: Three glacial modes of North Atlantic circulation (adapted from Rahmstorf [52]). Going from top to bottom the intersections are representations of circulation during an interstadial, a stadial, and a Heinrich event.

The North Atlantic Current (NAC) is presently transporting heat from the equator to the northern latitudes. This makes NAC a major contributer of the heat flux to the northern part of the North Atlantic, which also results in a milder climate in northern Europe. During a D/O NAC passes through different modes of circulation. These modes are linked to the density driven Thermohaline Circulation (THC), which drives NAC. Three modes of circulation are shown in Figure 1.5. Interstadial circulation is similar to the present THC, with arctic bottom water forming in the northern regions. During the stadials THC is inhibited by the presence of sea ice, while during Heinrich events THC is shut down due to influx of fresh water from ice bergs.
The glacial-interglacial cycle has a period of approximately 100.000 years. This 100.000 year cycle has been pronounced during the past million years.

The cycle is explained by variations in the Earth's orbital parameters, affecting the insolation recieved on Earth (Hays et al. [25]).

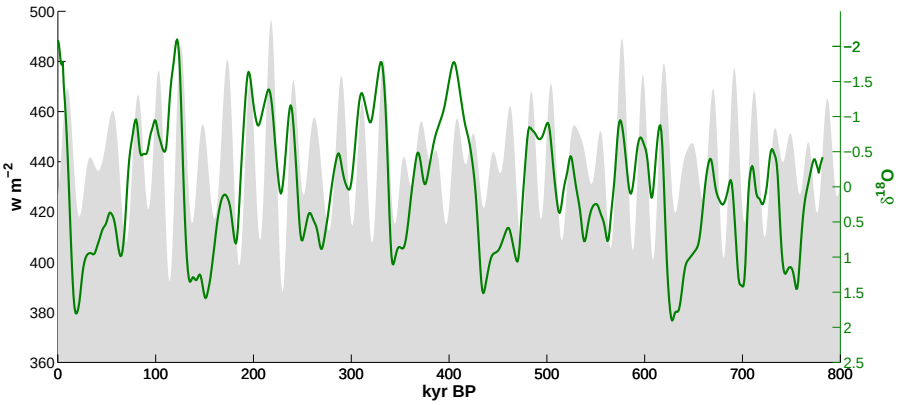

Figure 1.6: The shaded area is variations in insolation in July at 65°N (Berger [2]), while the green curve is stacked normalized planctonic $\delta^{18}O$ (Imbrie et al. [29]) from marine cores indicating variations sea surface temperature.

This connection between variations in insolation and Earth's climate, is shown in Figure 1.6. The summer insolation at the mid to high latitudes is important for the build up and decay of ice sheets. If the summer is not warm enough to melt the winter snow, the possibility of building ice sheets exists. However, this also depends on the amount of annual precipitation.

1.2.2 The Glacial Environment

During the last glacial massive ice sheets were accumulated on the North American and Eurasian continent (see Figure 1.7). The large amounts of water stored in ice sheets on land caused the sea levels to be depressed by 120m (Peltier [50]). The largest ice sheet on the northern hemisphere was the Laurentide Ice Sheet (LIS) in North America. The LIS was during LGM approximately the size of present day Antarctica.
The lower sea level, higher wind speeds and a general lower rate of precipitation resulted in a higher dust content in the atmosphere. This is observed as a higher dust content in the glacial parts of the ice cores (Hammer et al. [24]).
Cold polar air reached further south during the glacial. This can also be seen in estimates of the glacial sea surface temperature (SST).

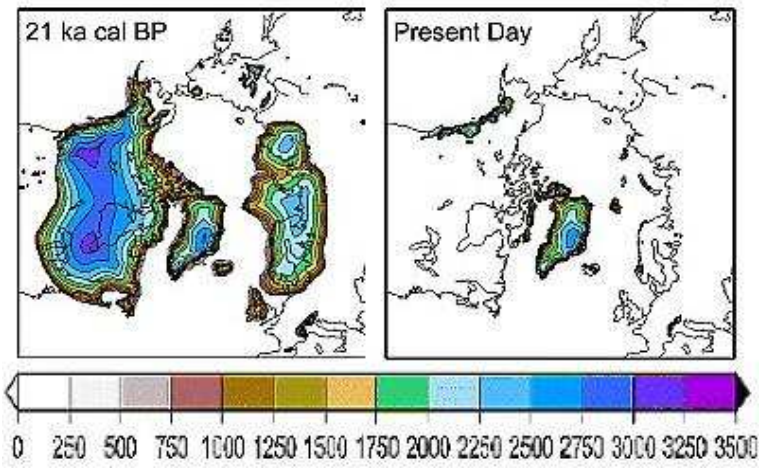

Figure 1.7: Modeled ice extent of the large ice sheets on the northern hemisphere during LGM compared to present ice sheets (adapted from Zweck & Huybrechts [66]). The bar is a scale in meters of the elevation of the ice sheet surface.

The oceanic polar front, which is an analogue to the atmospheric polar front[3], marks the transition from cold polar to warmer subtropical water. This is also the limit for winter sea ice. As seen in Figure 1.8 the oceanic polar front extended as far as the east coast of the Iberian Peninsula, which gives an impression of the glacial climate.

[3]A description of the atmospheric polar front is given in Section 2.2.

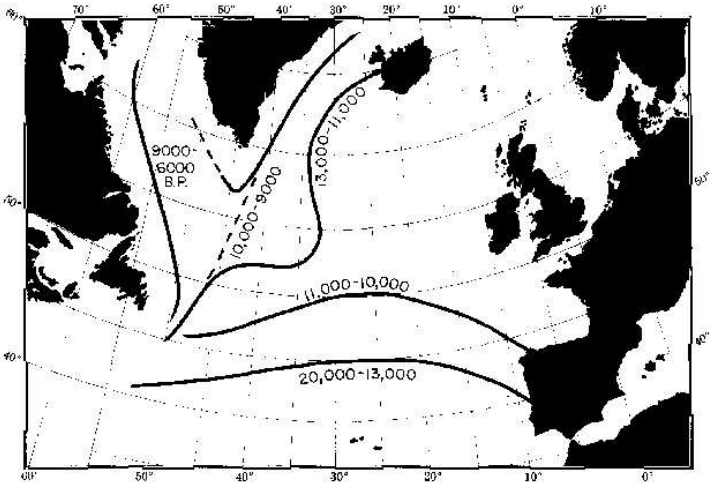

Figure 1.8: Estimates of the placement of the oceanic polar front in periods during LGM and the transition to Holocene (adapted from Ruddiman & McIntyre [56]).

Chapter 2

Meteorology

Modeling of the isotopic composition of precipitation involves basic meteorological calculations. This chapter is a presentation of the meteorological equations and knowledge needed to construct a simple isotope model.

2.1 Basic Equations

In the troposphere an air parcel can be cooled directly in two ways: By radiating heat isobarically or during adiabatic lifting of the parcel. During the lifetime of a low pressure system any cooling of the air will happen through these two processes.
An air parcel can also be cooled through mixing with air, that is lower in temperature than the parcel itself. This mechanism will not be considered here.

2.1.1 Adiabatic Cooling

When an air parcel is displaced vertically in the troposphere the temperature will change according to the vertical lapse rate. Under dry conditions the temperature will only depend on the heat capacity of dry air, while under wet conditions the heat capacity and any condensation of water vapor must be taken into account. Any cooling or heating is assumed to happen under adiabatic conditions, that is, no heat enters or leaves the parcel.
A useful approximation for wet adiabatic conditions is to assume that no liquid water is present in the parcel, which means that all droplets are precipitated as soon as they are formed. Quoting Byers ([9], p.8): *Physically, this is a preposterous assumption, but in the thermodynamic calculation it*

does not distort the result. The process under the assumption of immediate precipitation of condensate is a so called pseudoadiabatic process. The equation governing this process is as follows (Byers [9]):

$$c_p dT - \frac{RT}{m}\frac{dp}{p} + L dw_s = 0 \tag{2.1}$$

The first term of (2.1) is the contribution of dry air, with heat capacity c_p and the change of temperature dT. The second term is due to the pressure change dp, where p is pressure, T temperature, m molecular weight of dry air, and R is the gas constant. The last term is the heat contribution of condensation of water vapor, where L is the latent heat of evaporation and dw_s is the change of the mixing ratio, which is the specific water content of the air parcel. Equation (2.1) can be used to obtain the pseudoadiabatic lapse rate that is usually written

$$\frac{dT}{dz} = -\frac{g}{c_p}\frac{\left(1 + \frac{mLw_s}{RT}\right)}{\left(1 + \frac{Lw_s}{c_p dT}\frac{de_s}{e_s}\right)} \tag{2.2}$$

this expresses the change of temperature with height (details are given in Appendix A.2). Equation (2.2) is a valid approximation for describing the lapse rate under wet adiabatic conditions when no ice is formed. During the formation of ice crystals the air will be supersaturated with respect to the saturation vapor pressure over ice. Under such conditions an expression similar to equation (2.2) exits (see Appendix A.2 for details).

2.1.2 Isobaric Cooling

The Earth's atmosphere loses heat through long wave radiation to space. The process can be described isobarically for an air parcel. During isobaric cooling the parcel will act approximately as a black body, radiating heat at a given temperature. The amount of heat lost to space dq, can be expressed as

$$dq = -c_p dT - L dw_s \tag{2.3}$$

so apart from the actual cooling any heat gained by the parcel during condensation must also be taken into account. Equation (2.3) is basically the same as equation (2.1), except that heat is radiated to space instead of being converted to pressure changes, which is associated with vertical movements. As for the pseudoadiabatic lapse rate the heat capacity of any liquid water can be neglected.

2.1.3 The Water Content of Moist Air

The most important parameter determining the amount of water vapor in an air parcel is temperature. A relationship between temperature and water content can be expressed by the vapor equation:

$$e_s = e_{so} \exp\left(\frac{m_w L}{R}\left(\frac{1}{T_o} - \frac{1}{T}\right)\right)$$

which is based on the assumption of chemical equilibrium between liquid water and water vapor (see Appendix A.1 for details). Used in this context the vapor equation is an approximation, but it can be used with good results for meteorologic applications.

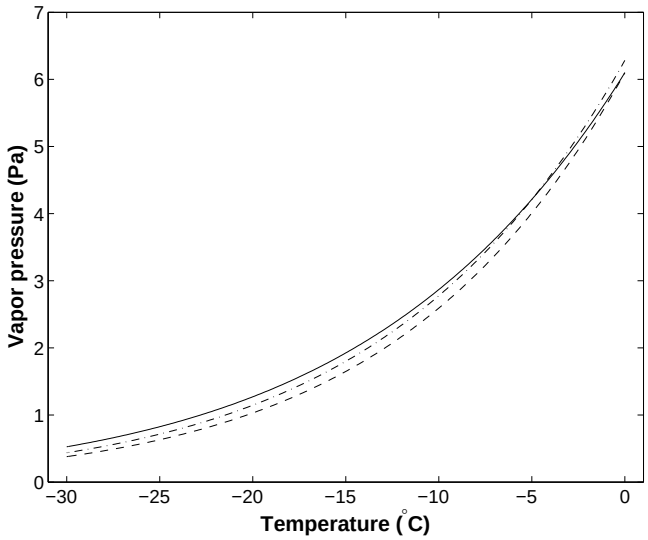

Figure 2.1: The vapor pressure plotted against temperature calculated using the vapor equation (A.2). The full line is the saturated vapor pressure with respect to water, the dashed line is the saturated vapor pressure with respect to ice and the dot-dashed line is the supersaturation pressure with respect to ice. The supersaturation is calculated using a simple linear parameterisation (defined in equation (4.2)).

The water content of moist air does not only depend on temperature, also cloud processes play an important role. One would naturally assume condensation to initiate as soon as the air is saturated with vapor. But because of micro physical processes during droplet and also ice formation,

some degree of supersaturation is usually necessary (see Section 2.4).
Water clouds usually have less than 1% of supersaturation, while ice crystals demand a higher level of supersaturation. The formation of ice crystals happens under conditions supersaturated with respect to ice, with the vapor pressure being intermediate between saturation with respect to water and ice. Supersaturation of $10 - 20\%$ are not unusual in ice clouds.
The water vapor pressure is shown in Figure 2.1 as a function of temperature. One should note the dramatic declination of vapor pressure with temperature, with the vapor pressure being 10 times lower at $-30°C$ compared to the vapor pressure at $0°C$. As it will be shown in Chapter 3, this is most important for the fractionation processes governing the isotopic content of precipitation.

2.2 The General Circulation

Circulation in the troposphere is generally controlled by unequal heating of the Earth's surface, caused by differences between the continents and oceans, and the low latitudes receiving more energy from the sun than the high latitudes.
The meridional circulation is characterised by vertical movements driven by buoyancy. That is, the rising of warm air and the subsidence of relatively cool air. The traditional view is the atmosphere being separated into multiple convective cells. This theory was introduced by Hadley [23], when trying to explain the origin of the westerlies.

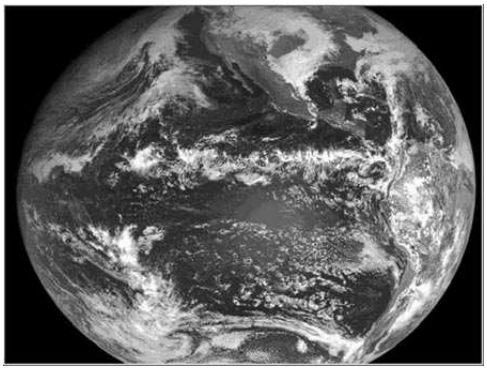

Figure 2.2: Image from the geostationary weather satelite Meteosat. The narrow cloudy band crossing the Pacific close to the equator is cumulus clouds forming in the the ITCZ.

The mechanism for convective cells can be described like this. Buoyancy causes warm air to rise. The air proceeds to the north and is gradually cooled. At some point the density, controlled mainly by temperature, will exceed that of the surroundings causing the air to sink. The cell is completed by air replacing the rising air initiating the circulation. This type of circulation is known as Hadley circulation.
Each hemisphere has three convective cells, the most pronounced one, which is located near equator, is denoted the Hadley cell. The driving force of this cell is a band of strong convection of warm moist air from both hemispheres associated with formation of cumulus clouds. This is known as the Inter Tropical Convergence Zone (ITCZ) (see Figures 2.2 and 2.3). The ITCZ is placed where the air masses from the northern and southern hemisphere converge, which is not exactly on the equator, but slightly to the north due to the distribution of land masses (Salby [57]).

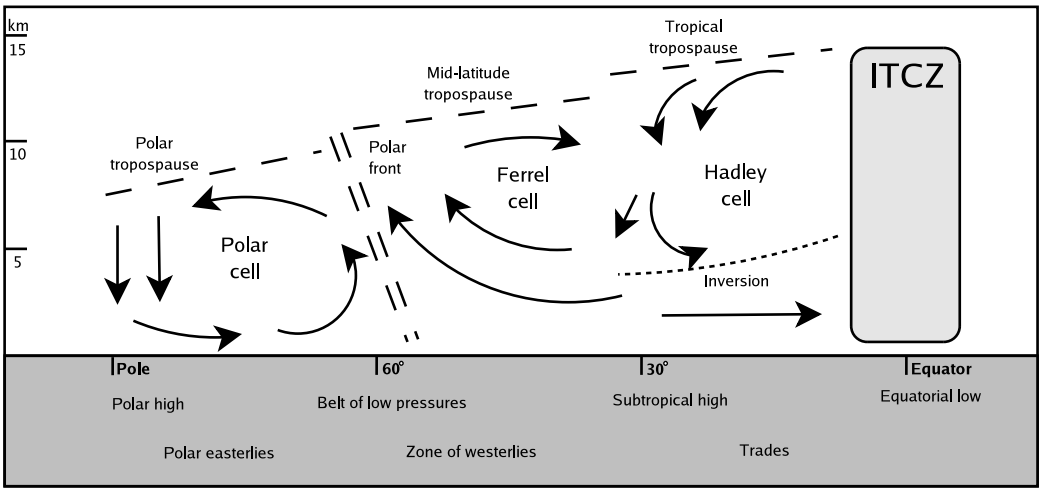

Figure 2.3: Schematic vertical section of the meridional circulation from equator to pole, with the major features of wind patterns and pressure noted (inspired by similar figure in Perry & Walker [51]).

In the polar region cold air subsides bringing down air masses from higher altitudes. The circulation in the polar cell is much weaker than in the Hadley cell due to less energy being available[1]. Intermediate between the polar and the Hadley cell, is the Ferrel cell, which acts as a link between the polar

[1]The Hadley circulation driven by convection in the ITCZ is fed by the release of latent heat (Salby [57]).

and the equatorial circulation. This cell is less defined and the circulation patterns less obvious.
An important feature of the midlatitudes is the separation of cold polar air from the warm subtropical air. This separation is performed by the polar front (see figure 2.3), which is associated with the formation of cyclones and anticyclones dominating the weather in this region. The placement of the polar front varies during the year. During the winter the front advances to the south, and retreats again in the summer.
So far, only the meridional component of the circulation has been described. The zonal component arises because of the fictious Coriolis force caused by the Earth's rotation. This deflects air currents to the right in the northern hemisphere and to the left in the southern. Together with the meridional cell structure this creates the alternating general wind patterns as the esterlies and westerlies (see notes Figure 2.3).

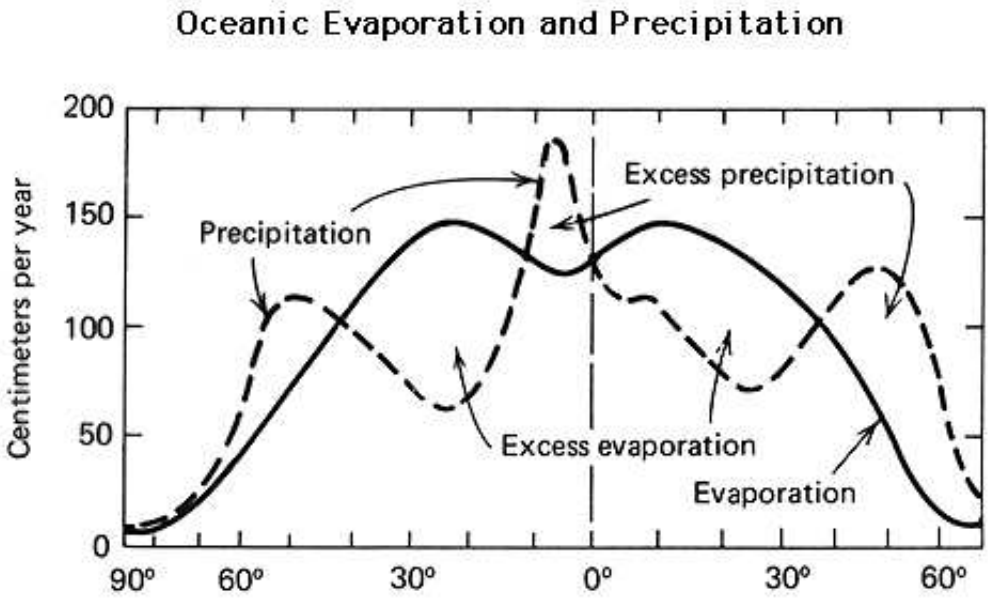

Figure 2.4: The global latitudinal variation of evaporation and precipitation. *Figure provided by Columbia University Department of Earth and Environmental Sciences from their Web page at http://www.ldeo.columbia.edu/edu/dees/ees/climate/slides/ocean_ep.gif.*

The cell structure of the atmosphere also affects the patterns of evaporation and precipitation. In the zones of generally upward moving air masses precipitation is likely to be formed as the air cools adiabatically and reaches

saturation. As opposed to this regions where the air subsides are generally more dry. Looking at the circulation patterns in Figure 2.3 one can explain the precipitation patterns in Figure 2.4, as the zones of the highest level of precipitation coincides with the regions of rising air around the equator and the polar front. These are also the regions of moisture surplus compared to the regions around 20° where also many of Earth's large deserts are located. The precipitation surplus of the midlatitudes and polar regions leads to the conclusion that some of the moisture must originate elsewhere. The obvious source of additional moisture for the high latitudes being the evaporative surplus of the subtropics.

2.3 Cyclones

The development of cyclones in the zone of the polar front is important for the transport of moisture to the high latitudes including Greenland. The polar front is not a stationary defined front, but is subject to high variability and depends on the momentary state of the atmosphere and ocean. The frontal zone may be more or less coherent, and wave structures linked to cyclogenesis[2] often develop.

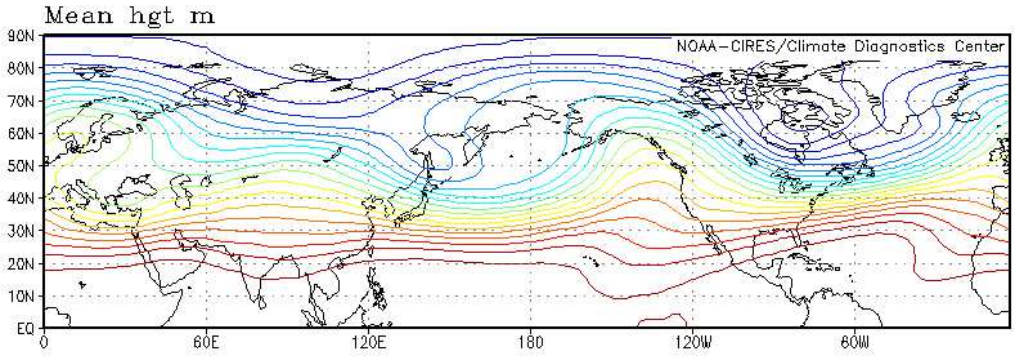

Figure 2.5: The mean 500mb geopotential height for the northern hemisphere, Febuary 2003. Maximum height is 5887.93m, and minimum height is 4932.36m. Contours are for every 50m. *Image provided by the NOAA-CIRES Climate Diagnostics Center, Boulder, Colorado, from their Web site at http://www.cdc.noaa.gov/.*

[2] Cyclogenesis is the development or intensification of cyclones.

Zones of strong meridional temperature gradients are linked trough the thermal wind balance to the development of strong upper level jets in the zonal direction (see Appendix A.3.1 for details). The thermal wind balance causes an intensification of the wind with altitude, which is the source of the polar jet stream. Jets are unstable[3] with respect to small pertubations and disturbances will amplify with time (Holton [27]). This results in wave structures in the upper level flow (see Figure 2.5).
The wave structures give rise to vertical movements and the initiation of cyclogenesis (see Appendix A.3.2 for details). Cyclones pick up moisture as they develop and eventually become occluded, separating parts of the initial air mass from the surface. The path of the cyclone will follow the general upper level flow along the jet stream.

2.4 Cloud Physics

A major feature of Earth's climate system is the presence of water clouds, which both reflect incomming radiation from the sun but also acts as an insulator by inhibiting loss of heat from the Earth's surface.
Also in the hydrological cycle clouds play an important role acting as containers in low pressure systems, transporting moisture from the subtropical regions towards the poles. In the context of this study clouds should be considered, taking into account cloud processes that might induce changes in isotopic ratios. This includes phase changes as condensation, evaporation, deposition and sublimation.
Clouds can consist of small water droplets, ice crystals or a mixture of both. This depends on the temperature of the cloud, which generaly is a function of altitude. The formation of clouds happens in air close to being saturated with water vapor, allowing droplets to condense or ice crystals to form.

2.4.1 Cloud Formation

There are different modes of formation of water droplets in air, only some are relevant to explain the naturally occuring cloud droplets. The most simple way to view the formation of droplets is homogeneous condensation, where the droplets form through collision of water molecules in the moist air. However, because of the high free energy barrier, this form of condensation requires a supersaturation of several hundred percent, for droplet embryos to

[3]Baroclinic instability.

persist. This level of supersaturation is never obtained in nature because of other condensation prosesses requireing less humidity to form droplets (Mason [44], p. 20).
In actual clouds the condensation of vapor is initiated by aerosols which act as CCN (Cloud Condensation Nuclei). A CCN can be soluble or insoluble in water or a combination of both, with a insoluble core surrounded with a film of soluble substance.
In the case of a soluble CCN the condensation can initiate at a lower degree of supersaturation compared to homogeneous condensation. This is because of the fact that the vapor pressure over a solution is lower than over a pure solvent, which is true except for a few irrelevant cases (Byers [9]). The lower vapor pressure prevents the droplet embryos from evaporating, allowing the growth of the droplet to continue to reach a stable size. The soluble CCN requires the least degree of supersaturation to initiate condensation.
For the insoluble CCN the effect on the nucleation proces is to lower the free energy barrier compared to homogeneous condensation, with the effect depending on the geometry of the CCN (Mason [44], p. 20 *ff.*). Insoluble CCN requires a moderate supersaturation to initiate condensation.
The CCN mentioned above as being a combination of soluble and insoluble are often found in nature, when the relative humidity is above 70%. These CCN act as soluble with respect to the degree of supersaturation required to initiate condensation (Mason [44], p. 29).
The chemical composition of CCN varies geographically with the distance from the sources. Important substances as $NaCl$ and SO_2[4] can be mentioned. The main source of $NaCl$ is air bubbles bursting in the foam of breaking waves of sea water, producing a small jet of fine droplets. The source of SO_2 is mainly continental, being forest fires and volcanoes (Mason [44], p. 68). Apart from these natural sources human activities of course play a role in the present production of aerosols.

2.4.2 The Ice Phase in Clouds

The formation of ice crystals in clouds is parallel to the condensation proces described above with respect to the prescence of a nuclei to initiate the proces. Direct deposition of water vapor to ice is very difficult to obtain, but it has been done experimentally (Byers [9]). Also the fact that pure water drops can be cooled to $-40°$C before spontaneous freezing occurs points towards a crystallization proces in clouds which involves impurities to initiate.

[4] SO_2 oxidizes to SO_3, which reacts with water to form H_2SO_4.

The initiation of the ice phase depends on the nature of the Ice crystallization Nuclei (IN) and the type of crystallization proces. Different IN will become active at different temperatures, and each kind of IN can be assigned a specific activation temperature. As opposed to CCN the most effective IN is highly insoluble[5] in water and is often composed of wind blow dust originating from arid regions of the continents. The rate of formation of ice crystals is affected by the number of IN present, and the size distribution of the IN.
Four different modes of crystallization have been suggested, all of which involves the prescence of an IN (Vali [63]):

Deposition

During deposition water molecules settle of the surface of the IN to form ice crystals without prior condensation. This process involves diffusion of water molecules from the ambient moist air to the surface of the IN. The air must be supersaturated with respect to ice.

Immersion Freezing

If an IN is present in an existing water drop, the droplet will freeze if it is cooled and reaches the activation temperature of the IN.

Condensation Freezing

This proces requires supersaturation with respect to water and the temperature to be below the activation temperature of the IN. Water vapor condenses onto the IN and then freezes.

Contact Freezing

If an exisisting supercooled water droplet collides with an IN and the temperature is below the activation temperature of the IN, the collision will cause the droplet to freeze.

For each of the initiation modes the activation temperatures are likely to be different even using the same type of IN. Some experiments have been done trying to quantify the difference between the initiation modes but further research is needed (Vali [63]).
However, extensive experimentation with cloud chambers have been exercised

[5]The prescence of a substance soluble in water such as salts, will lower the freezing point of water (Mason [44], p. 190). The most obvious example being that sea water has a freezing point below 0°C.

during the past fifty years to obtain the ice nucleating abilities of different substances. A few results are listed in Table 2.1.

Substance	Activation temperature (°C)
Silver iodide	-5
Kaolinite	-9
Illite	-9
Gypsum	-16

Table 2.1: Ice crystallization nucleis and their experimentally obtained activation temperatures (Mason [44], p. 196-197). Substances are naturally occuring IN except silver iodide, which is used for artificial cloud seeding.

Of particular interest to this study is kaolinite and illite. These two clay minerals have been found in central Greenland ice cores comprising a significant fraction of the dust, with illite being the most abundant (Bory et al. [5]). This could give a hint to answer the question of the ice phase initiation temperature in the clouds that form the central Greenland precipitation.
The dust present in the ice cores will either have undergone wet or dry deposition. In the case of wet deposition, there is a possibility of the dust acting as IN. With illite being the most abundant mineral, the best guess of an initiation temperature for the central Greenland precipitation, would be the activation temperature of illite.
However, further complications might compromise this simple interpretation. If an IN has been activated and participated in the formation of an ice crystal, but the ice has sublimated under conditions with low humidities and higher temperatures, then the IN is said to be preactivated. This results in higher activation temperatures. In the case of kaolinite activation temperatures of -4°C has been achieved by preactivation (Mason [44], p. 191). The most likely explanation for this memory effect is retention of ice embryos in capillaries in the surface of the IN (Vali [63]).

2.4.3 Mixed Cloud Processes

As a consequence of water droplets in clouds having no fixed freezing point, there is a possibility of clouds having both ice and supercooled water droplets in the same cloud layer. In 1911 Wegener [64] suggested a mechanism for growth of ice crystals in mixed phase clouds.

In an enviroment with both ice crystals and water droplets the vapor pressure will adjust so it is intermediate between that of water and ice. In such an environment the vapor will be supersaturated with respect to ice and subsaturated with respect to water. Thus, the water droplets will have a tendency to evaporate, and the ice crystals will grow at the expense of the water droplets.
Wegeners mechanism was later described by Bergeron [3] and adopted by Findeisen [20], and is widely know as the Bergeron-Findeisen process. The process has been confirmed to actually take place in the atmosphere, and must be taken into account when describing cloud processes (Strickley [62]).

Chapter 3

Isotopic Fractionation

The mechanisms of isotopic fractionation during the phase changes of water is presented in this chapter. This is the basis for modeling the isotopic changes of precipitation.

3.1 Equilibrium Fractionation

The fractionation of the isotopic components of water during phase transition between vapor/liquid or vapor/solid arises because of differences in vapor pressure (denoted e for light and e' for heavy components). The heavier components have a lower vapor pressure i.e. they will evaporate slower and condense more readily than the lighter components. From a thermodynamic point of view the differences in vapor pressure exists because of different chemical potentials of the isotopic components.
The fractionation process is described through the use of a fractionation factor α. Under equilibrium conditions α will be equal to e/e' for evaporation when defined through

$$R_c = \alpha R_v \tag{3.1}$$

where R_c and R_v is the isotopic ratio of the condensate and vapor, respectively.

3.1.1 Rayleigh Condensation

The isotopic changes in the vapor of an air parcel during condensation can be described by Rayleigh condensation (Dansgaard [16]). In this type of condensation all condensate is removed from the parcel as soon as it is formed.

If the initial vapor has the isotopic ratio R_v and the mixing ratio w_s, then the change during condensation can be written as

$$R_v w_s = (R_v + dR_v)(w_s + dw_s) - R_c dw_s \tag{3.2}$$

The first term on the right expresses the isotopic ratio and mixing ration of the vapor after condensation of dw_s of vapor. The second term on the right is the amount of condensate dw_s with the isotopic ratio R_c. By leaving out all second order terms and using Equation (3.1), Equation (3.2) simplifies to

$$0 \cong R_v dw_s + w_s dR_v - \alpha R_v dw_s \tag{3.3}$$

Rearrangeing Equation (3.3) leaves us with a differential expression for the change in the isotopic ratio of the vapor during condensation

$$\frac{dR_v}{R_v} = (\alpha - 1)\frac{dw_s}{w_s} \tag{3.4}$$

A similar equation can be found for the condensate by using $dR_c = d(\alpha R_v) = d\alpha R_v + dR_v \alpha$ and Equation (3.4)

$$\frac{dR_c}{R_c} = (\alpha - 1)\frac{dw_s}{w_s} + \frac{d\alpha}{\alpha} \tag{3.5}$$

3.2 Kinetic Effects during Evaporation and Deposition

Equilibrium fractionation only explains part of the fractionation observed during evaporation and deposition, thus non-equilibrium or kinetic effects must be taken into account.

3.2.1 Fick's Law

An important tool in describing diffusional processes is the postulate, that the flux of molecules to a plane is linearly related to the gradient of the concentration of the substance in question. This relationship is known as Fick's law. Fick's law was first used in molecular diffusion theory, but has since been used in analogy in parameterizations of turbulent diffusion. Fick's law is often written as

$$F = -D_* \nabla C' \tag{3.6}$$

where F is the flux of molecules, D_* is the diffusivity and C' is the concentration of a given substance.

3.2.2 Boundary Layer Diffusion

When water evaporates from the ocean the layer closest to the surface will be saturated with vapor and the proces can be described by equilibrium fractionation. When reaching the turbulent boundary layer the air will no longer be saturated with vapor, and the fractionation will be affected by a number of factors like relative humidity, wind speed and the diffusivities of the isotopic components of water (see also Figure 3.1).
A model for isotopic fractionation during evaporation has been developed by Merlivat & Jouzel [48]. In the model steady state is assumed for the isotopic components of water, so that

$$\delta_e = \delta_{vo} \tag{3.7}$$

where δ_e is the isotopic composition of the evaporative flux from the ocean, and δ_{vo} is the initial isotopic concentration of the vapor in the moist air mass, for either D or ^{18}O.
The evaporation flux at the top of the boundary layer E can be written in analogy with Equation (3.6) as

$$\frac{E}{\rho} = \Gamma \frac{(w_s - w)}{z} \tag{3.8}$$

where ρ is the air density, w_s is the mixing ratio in the saturated layer just above the sea surface, w is the mixing ratio at the top of the boundary layer, z is the thickness of the boudary layer and Γ expresses the effective diffusivity, which includes both turbulent and molecular diffusion.
The isotopic analoge to Equation (3.8) is given by

$$\frac{E_i}{\rho} = \Gamma_i \frac{(w_{si} - w_i)}{z} \tag{3.9}$$

with

$$w_{si} = R_s w_s$$

$$w_i = R_v w$$

As the isotopic concentration of each isotopic species must be proportional to the flux of the species, the isotopic ratio at the top of the boundary layer can be written as the ratio between the fluxes

$$R_e = \frac{E_i}{E} \tag{3.10}$$

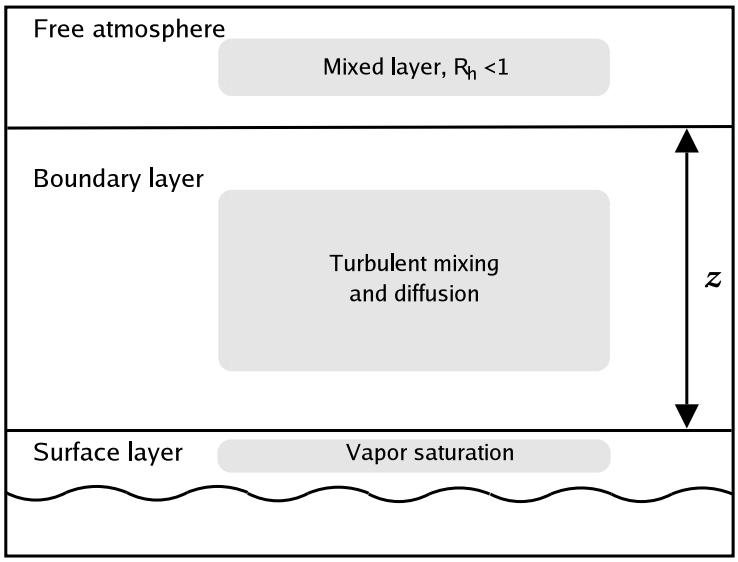

Figure 3.1: Schematic representation of the zone, where evaporated water from the ocean is exchanged with the atmosphere. The characteristics of each layer is noted in the gray boxes.

Or using the δ notation and combining Equation (3.8), (3.9) and (3.10)

$$1 + \delta_e = (1 - k)\frac{1/\alpha - R_h(1 + \delta_{vo})}{1 - h} \tag{3.11}$$

with $k = 1 - \Gamma_i/\Gamma$ and the relative humidity $R_h = w/w_s$. When using the steady state assumption in Equation (3.7) a relation for the initial isotopic concentration of the vapor can be derived

$$\delta_{vo} = \frac{1}{\alpha}\frac{1 - k}{1 - kR_h} - 1 \tag{3.12}$$

The value of k in Equation (3.12) depends on the wind speed, so a rougher wind regime will give a higher degree of fractionation (Brutsaert [8], [7]). The ocean is considered to be smooth, which gives the value of k to be $6‰$ for $H_2^{18}O$.

3.2.3 Kinetic Effects during Deposition

In the polar regions snow is likely to form through deposition, where ice crystals form directly from the vapor phase. Deposition happens under supersaturated conditions with respect to ice and requires low temperatures

to initiate (see section 2.4.2). Because of differences in diffusivities in air of the isotopic components of water, the heavy components will deposite slower than the main component $H_2^{16}O$. This has been described by Jouzel & Merlivat [36] through the equations presented below.
According to Equation (3.6) the flux of molecules to a plane surface will be proportional to the diffusivity D_*, and the difference between partial pressure e_v and saturation vapor pressure over ice e_i, when assuming the proces is purely molecular or non-turbulent. So we may write

$$F \propto D_*(e_v - e_i) \tag{3.13}$$

The ratio between the vapor pressure of the heavy and light isotopic components must be equal to the ratio of the isotopic concentrations, that is

$$\frac{e'_v}{e_v} = R_v \tag{3.14}$$

$$\frac{e'_i}{e_i} = R_s \frac{1}{\alpha} \tag{3.15}$$

where the vapor pressures for the heavy components are written with primed symbols, R_v and R_s are the isotopic concentrations for the vapor and solid, respectively, and α is the equilibrium fractionation factor. Written in terms of δ Equation (3.14) and (3.15) becomes

$$e'_v = e_v R_{SMOW}(1 + \delta_v) \tag{3.16}$$

$$e'_i = e_i R_{SMOW}(1 + \delta_s)/\alpha \tag{3.17}$$

where R_{SMOW} is the isotopic ratio of standard mean ocean water, δ_v and δ_s is the isotopic composition of the vapor and the condensate at the surface, respectively.
The isotopic composition of the condensate δ_s is governed by the fluxes of the heavy and main components denoted F' and F respectively

$$1 + \delta_s = \frac{1}{R_{SMOW}} \frac{F'}{F} \tag{3.18}$$

or using Equation (3.13), (3.16) and (3.17)

$$1 + \delta_s = \frac{D'_*}{D_*} \frac{(e_v(1 + \delta_v) - e_i(1 + \delta_s)/\alpha)}{(e_v - e_i)} \tag{3.19}$$

which simplifies to

$$1 + \delta_s = \alpha_k \alpha (1 + \delta_v) \tag{3.20}$$

with

$$\alpha_k = \frac{S_i}{\alpha D_* / D'_* (S_i - 1) + 1} \tag{3.21}$$

S_i is the supersaturation with respect to saturation vapor pressure over ice. S_i is defined

$$S_i = \frac{e_v}{e_i} \tag{3.22}$$

As seen from Equation (3.21) the supersaturation is an important factor controling the fractionation proces.
If $S_i = 1$ the fractionation will be an equilibrium proces controlled only by the temperature dependence of α. When increasing the supersaturation the fractionation will gradually become more dominated by diffusion.

3.2.4 Diffusivities and Fractionation Factors of the Isotopic Components of Water

From Equation (3.6) it is clear, that the diffusivity will be an important factor in determining the flux of molecules during a diffusional proces. The diffusivity expresses the ability of a molecule to be displaced through a substance. In this case we are interested in the diffusivities of the isotopic components of water vapor in atmospheric air[1].
Past experiments have shown that the diffusivities of the isotopic components of water vapor did not fit the usual kinetic theory without additional effects affecting the proces. The experiments have been carried out with water evaporating in an unsaturated enviroment. Merlivat [47] proposed that differences in the molecular collision diameters were affecting the diffusion. With the diameters Γ, being ordered as

$$\Gamma_{H_2^{18}O} < \Gamma_{H_2^{16}O} < \Gamma_{HD^{16}O}$$

However there is little solid evidence of the diameters being ordered as this, and that it should affect the diffusivities in any significant way (Cappa et al. [10]).

[1]Experiments are usually carried out in nitrogen.

Recent work by Cappa et al. [10] show a different approach in determining the diffusivities. During evaporation a skin layer of water is cooled, and a temperature gradient will persist in the top few milimeters of water. The cooling is significant enough to affect the fractionation proces, as the equilibrium fractionation factor α, depends on temperature (see Figure 3.2). When taking the effect of the cooling into account the diffusivities can be explained by kinetic theory, resulting in different diffusivities than obtained by Merlivat.
As mentioned above α depends on the temperature of evaporation. α can be found experimentally to satisfy the Equations (3.23) and (3.24) for $HD^{16}O$ and $H_2^{18}O$ respectively (Majoube [43]).

$$\alpha_D = \exp\left(\frac{24844}{T^2} - \frac{76.248}{T} + 52.612 \times 10^{-3}\right) \tag{3.23}$$

$$\alpha_{^{18}O} = \exp\left(\frac{1137}{T^2} - \frac{0.4156}{T} - 2.0667 \times 10^{-3}\right) \tag{3.24}$$

In Figure 3.2 the fractionation factors are plotted for a temperature range. This show that α_D varies more with temperature than $\alpha_{^{18}O}$. Consequently the relationship between $\delta_{^{18}O}$ and δ_D will be affected by the temperature of evaporation. The deuterium excess d, will thus also be affected depending on the evaporation temperature.

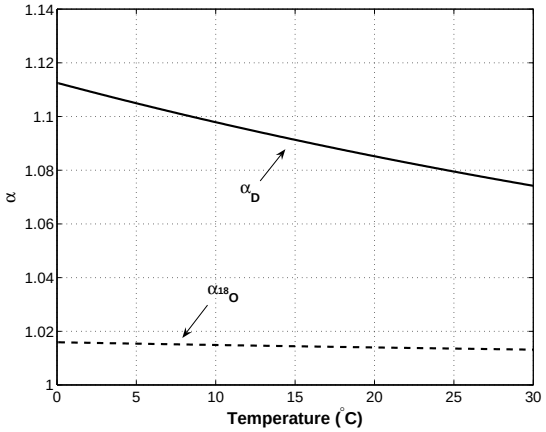

Figure 3.2: Fractionation factor α for $[^{18}O/^{16}O]$ and $[D/H]$ marked by the dashed and full line, respectively.

Chapter 4

The Model

To model the isotopic composition of Greenland precipitation a simple Rayleigh-type fractionation model is used. The model is a modified version of the one used by Johnsen et al. [35]. The original model is hereafter denoted model I and the modified current one, model II.
Model I and model II are basically very similar and the general structure of the models is the same. The differences between the two models are pointed out in Section 4.2.1.

4.1 Model Description

The goal is to simulate the transport of an air parcel, from the point where the parcel receives water vapor from a source of evaporation to a site on the Greenland ice sheet. The source of evaporation is assumed to be located in the North Atlantic. During the transport to the ice sheet the isotopic composition of the water vapor and precipitation is calculated.

4.1.1 The Trajectory

There are two fixed locations in the trajectory. One is the source of evaporation, and the other is the site of deposition in Greenland. In between the fixed locations the trajectory is described in terms of elevation and temperature. The zonal component of transport is not considered. The parcel begins the trajectory with a prescribed temperature and humidity, and is then cooled, assuming that the parcel is being transported to the north.
At some point the parcel enters a cyclonic system, and as a part of the vertical movements in such systems the parcel will be transported upwards. During

the ascent the parcel will be cooled in accordance with the pseudoadiabatic lapse rate (details in Section 2.1.1). The cyclone follows a track to Greenland and during this northward movement the parcel cools isobarically (details in Section 2.1.2). The combination of isobaric and pseudoadiabatic cooling will continue until the parcel reaches the edge of the ice sheet. From this point the parcel will ascend to the site, being cooled only pseudoadiabatically.
The model is constructed in such a way that the trajectory is determined by the initial conditions at the source and the $\delta^{18}O$ value at the site, which is an input parameter to the model. The trajectory consists of a number of alternating isobaric and pseudoadiabatic steps (see Figure 4.1). After one isobaric and one pseudoadiabatic step, the model lifts the parcel pseudoadiabatically to the site and tests if the precipitation has reached the correct $\delta^{18}O$ value. The model repeats this procedure until the site $\delta^{18}O$ value is obtained. In this iterative manner the parcel may reach a location in southern or northern Greenland, depending on the site $\delta^{18}O$ value.

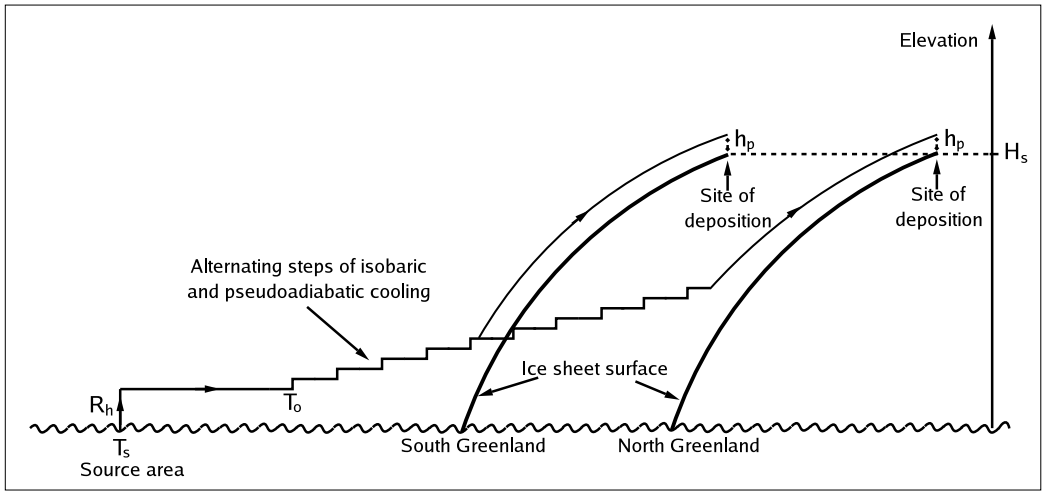

Figure 4.1: Illustration of the moisture transport from the source area to the Greenland site, as modeled by model I and II. Noted parameters are explained in Section 4.1.2 and 4.1.3.

4.1.2 Boundary Conditions

As mentioned above the trajectory is determined by the initial source conditions and the site $\delta^{18}O$ value. One can view this as the model boundary conditions.

At the source the initial air mass is characterized by the surface temperature T_s and the relative humidity R_h. Together these two quantities determine the dew point of the parcel, which determines the initiation of Rayleigh condensation. T_s and R_h are deciding factors on the initial isotopic composition of the vapor, but also affects the δ values of the precipitation at later stages. This will be discussed further in Section 4.2.3.
At the site the $\delta^{18}O$ value of the precipitation is prescribed as a model input. This determines the site temperature and moisture content of the parcel at the moment of condensation, as these are linked to the $\delta^{18}O$ value of the precipitation through Equation (3.4). Because the mean site $\delta^{18}O$ value is an input of the model, the cloud temperature and deuterium excess at the site are the parameters that we actually obtain through the calculation. This means that the model is bound by actual $\delta^{18}O$ measurements on the Greenland site.
The annual cycle of the isotopic values can be investigated by choosing $\delta^{18}O$ values that approximate an annual cycle on the site. According to Johnsen et al. [35] the monthly $\delta^{18}O$ values on Greenland can be approximated by

$$\delta_{pi} = \overline{\delta_p} - \Delta\delta_p \cos(2\pi(i - 1.5)/12) \tag{4.1}$$

where i refers to the month, $\overline{\delta_p}$ is the mean value for the annual precipitation at the site and $\Delta\delta_p$ is amplitude of the annual $\delta^{18}O$ cycle.

4.1.3 Model Parameters

The model has a number of parameters which can be adjusted to optimize the simulation: T_0, T_f, C, F, and ϕ.
T_0 decides at which temperature the parcel enters the cyclonic system, which means that the parcel commences pseudoadiabatic cooling. The choice of T_0 is of little importance as the impact of the trajectory on $\delta^{18}O$ at the site is relatively small. As long as T_0 is below the dew point, and is reached before the parcel reaches the edge of the ice sheet, the choice of T_0 is somewhat arbitrary.
The freezing temperature T_f, initiates the glacial regime of the air parcel. At temperatures below T_f all precipitation will be formed as snow. Therefore T_f also marks the onset of diffusion induced fractionation during deposition under supersaturated conditions, affecting the δ values of the precipitation.
In the model the parameterization of the supersaturation is adopted from Jouzel & Merlivat [36]. The supersaturation S_i is assumed to be described

by a linear function of the temperature cloud temperature T, so that

$$S_i = C - FT \tag{4.2}$$

where C and F are tuning parameters, that does not represent any real physical factors. C and F are determined through trial and error, tuning the model to the conditions at the site.
During the final ascend to the site the parcel is elevated above the ice sheet by the distance h_p, which is assumed to be given by

$$h_p = 500 + \phi(3200 - H_s) \tag{4.3}$$

where H_s is the site height. The factor ϕ is a tuning parameter to adjust the vertical gradient of $\delta^{18}O$. ϕ should be tuned so the vertical gradient matches the observed gradient of $-0.62‰$ per 100m (Johnsen et al. [35]). If the site is located in central Greenland, which has an elevation of 3200m, h_p will be equal to 500m.

4.1.4 Isotopic Fractionation

The vapor, which eventually deposits as snow on the ice sheet, has during its history undergone several processes changing the isotopic composition. Initially the δ value of the vapor is decided by the source conditions during evaporation, described with T_s and R_h.
T_s affects the fractionation because of the temperature dependence of the fractionation factor α. T_s also affects the fractionation indirectly as w_s generally varies with the temperature, and Rayleigh condensation depends on w_s.
The diffusional process during evaporation, described in Section 3.2.2 is included in the model. The process depends on R_h, with no diffusion driven fractionation if $R_h = 1$. Figure 4.2 shows how the initial deuterium excess in the vapor is affected by the source conditions.
When the parcel reaches dew point Rayleigh condensation is initiated. It is assumed that the water droplets form with no supersaturation. This is valid for water clouds. The cooling will continue with the parcel being on the point of saturation. During condensation the fractionation will be governed by Equation (3.4), which is integrated numerically.
The condensation of water vapor to droplets continues until T_f. After this the parcel enters the glacial regime. Precipitation will fall as snow and diffusion will affect the fractionation as described in Section 3.2.3. The deposition of vapor happens with the air being supersaturated with respect to ice. This

means that the vapor pressure will be intermediate between saturation with respect to ice and saturation with respect to water.

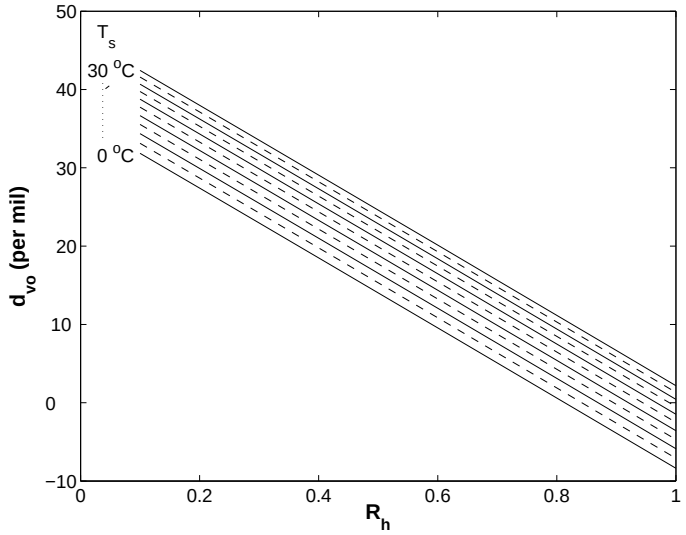

Figure 4.2: The deuterium excess d_{vo} in vapor evaporated with varying source temperature T_s and relative humidity R_h. T_s is varied from 0°C to 30°C in steps of 3°C.

At the T_f transition excess vapor has to be deposited to obtain the correct mixing ratio. The water content in the air now must follow the supersaturation with respect to ice, instead of saturation with respect to water. The deposition of the excess vapor releases energy to the parcel. This energy is assumed to lift the parcel pseudoadiabatically.
As the vapor deposits the S_i parametrization will control the diffusion induced fractionation, but it will also affect the lapse rate through the different mixing ratio caused by the supersaturation (see Equation (A.6) for details).

4.2 Modeling

This section will present examples of model runs simulating the isotopic composition of precipitation along trajectories to demonstrate the models behavior. The first step is to choose the model parameters, most importantly the freezing temperature T_f, and the supersaturation parameterization S_i. As a rule the diffusivities from Cappa et al. [10] are used unless other is indicated

(diffusivities are discussed in Section 3.2.4).
Following earlier modelers T_f is set to -5°C (Ciais & Jouzel [11], Johnsen et al. [35]). As discussed in Section 2.4.2 the exact T_f is highly dependent on micro physical processes. This makes the choice of T_f difficult. In this study the choice of T_f should be viewed as the point, where the ice phase in the cloud begins to affect the fractionation, rather than the complete glaciation of a cloud.
Another reason for choosing this T_f, is to ensure that the phase transition in the cloud, and the following change in fractionation, does not interfere with the simulation of low δ values. The model output for the Greenland site should not be directly affected by the choice of T_f.
The S_i parameterization has a strong effect on the site excess. S_i is tuned to match the present day annual mean excess values on southern and central Greenland sites. This is done by using source data from Weathership E (ship E 35°N, 48°W) (IAEA/WMO [28]), and running the model for the site $\delta^{18}O$ values, adjusting the S_i parameterization to match the excess. Ship E was found by Johnsen et al. [35] to be an adequate representative for the *main* moisture source for the precipitation in central Greenland.
The S_i tuning for Greenland site conditions found in this study is

$$S_i = 1.025 - 0.0033T$$

where T is the cloud temperature in °C.

4.2.1 Comparison between Model I and Model II

Figure 4.3 shows the excess d_p and $\delta^{18}O_p$ from numerous model runs with different source conditions. The suffix p indicates that it is the value for the precipitation. The starting point of each curve has $\delta^{18}O_p$ close to zero, which is the value for the dew point. This means that the condensation is initiated to the far right of the figure, and the simulation is terminated when $\delta^{18}O_p$ reaches approximately -50‰.
The curves all show a kink in the d_p–$\delta^{18}O_p$ relationship. This is the transition from condensation to deposition, and shows the effect of changing to the kinetic fractionation factor during deposition. Immediately after the phase transition in the cloud d_p is lower, and the slope of the curve drops, causing a high d_p at the end of the integration.
The bottom plot in Figure 4.3 illustrates the differences in simulations when using diffusivities found by Cappa et al. [10] and Merlivat [47]. For $\delta^{18}O_p$ values of 30–40‰, which is the range for present day central Greenland values, the d_p values are similar using the different diffusivities.

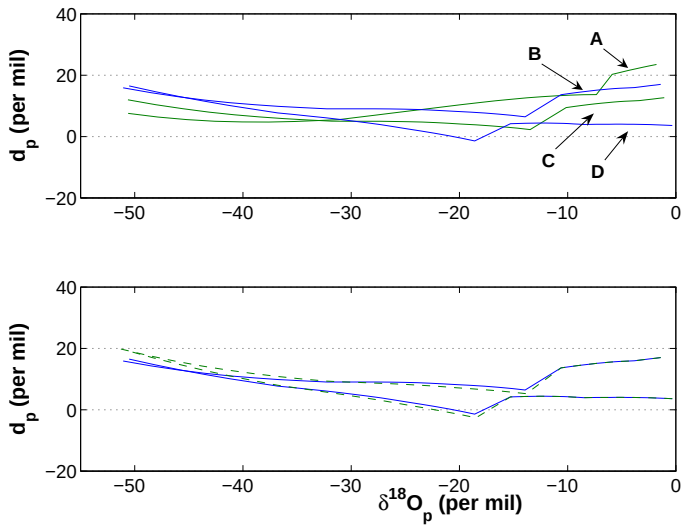

Figure 4.3: d_p plotted against $\delta^{18}O_p$. **Top**: Four model II runs each with different R_h and source temperature. Curve A: $R_h = 0.57$, $T_s = 12°\text{C}$, $w_{so} = 5g/kg$. Curve B: $R_h = 0.68$, $T_s = 20°\text{C}$, $w_{so} = 10g/kg$. Curve C: $R_h = 0.76$, $T_s = 18°\text{C}$, $w_{so} = 10g/kg$. Curve D: $R_h = 0.93$, $T_s = 26°\text{C}$, $w_{so} = 20g/kg$. **Bottom**: Curve B and D as above (full curve) but plotted together with model II runs (dashed curve) using diffusivities from Merlivat [47], but with same T_s and R_h as curve B and D.

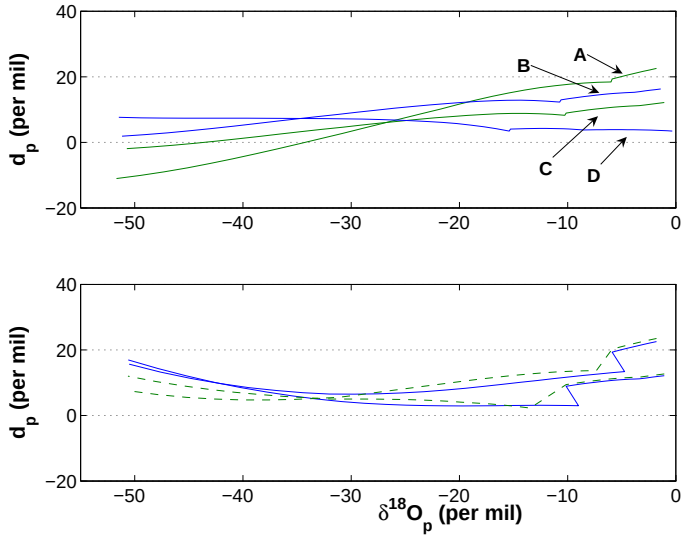

Figure 4.4: **Top**: Same as the top plot in Figure 4.3 but with calculations done with model I. **Bottom**: Curve A and C calculated with model I (full curve) and model II (dashed curve) both using the model II tuning $S_i = 1.025 - 0.0033T$.

For lower $\delta^{18}O_p$ values around -45‰ the differences becomes significant. This would lead to differences in interpretations when simulating the glacial $\delta^{18}O_p$ values.
The top plot in Figure 4.4 shows model I results for same initial conditions as for model II in Figure 4.3. The model is run with the Merlivat diffusivities and tuning for Greenland $\delta^{18}O_p$ values $S_i = 1.04 - 0.007T$, which is basically a reproduction of a plot from Johnsen et al. [35]. When comparing model I and model II the model results are qualitatively similar. Curve A has the highest initial d_p, but also the lowest site values, while Curve D has the lowest initial d_p and the highest site values. Curve B and C are approximately parallel.
The quantitative differences between the model results are partly due to different S_i tunings, and the use of different diffusivities. Apart from this the models do not describe the T_f transition similarly. One difference is, that model I does not account for deposition of excess moisture during the transition. There is also a typing error in the code for model I, which results in wrong fractionation factors for $H_2^{18}O$ during deposition. This also affects the d_p-$\delta^{18}O_p$ relationship after T_f has been reached.
Furthermore, there is an inconsistency in model I, when calculating the fractionation during deposition. The supersaturation is taken into account with respect to the isotopic calculations, but not in the meteorologic calculation. This affects the isotope values, as the fractionation is affected by the mixing ratio.
To compare the model results directly, it would be obvious to reproduce the model I results presented by Johnsen et al. [35] with model II, using the same S_i tuning. However, because of the different handling of the T_f transition by model I and II, it is not possible for model II to produce a meaningful result using the model I tuning. So we are unable to test the model I results directly with model II.
To illustrate the model differences, model I is therefore run with the model II S_i tuning, resulting in similar d_p-$\delta^{18}O_p$ curves as shown in the bottom plot in Figure 4.4. The main differences illustrated is the higher d_p for low $\delta^{18}O_p$ for model I, and the T_f transition for model I results in higher $\delta^{18}O_p$ values. The high d_p values can be corrected by changing the S_i tuning and does not tell us whether model I or model II is correct. However, the higher $\delta^{18}O_p$ values after the transition suggests that model I is not handling the transition correctly. During successive condensation/deposition the $\delta^{18}O_p$ is expected to get gradually more negative, also during a phase transition.

4.2.2 The Cloud Temperature and the Isotopic Composition of Precipitation

To investigate the relationship between temperature and isotopic composition of the precipitation, the condensation temperature in the cloud T_p can be plotted against $\delta^{18}O_p$. Johnsen et al. [35] found the relationship $T_p = 1.04\delta^{18}O_p + 10.6$ for site values using model I with ship E as source. A similar result can be obtained using model II also with ship E as source

$$T_p = (1.08 \pm 0.09)\delta^{18}O_p + (11.9 \pm 3.3) \tag{4.4}$$

These T_p-$\delta^{18}O_p$ relationships calculated by model I and II show a strong similarity in spite of model and model tuning differences. This implies that there exists a strong linear T_p–$\delta^{18}O_p$ relationship for central Greenland, which is approximatelty one-to-one (see also Figure 4.5).

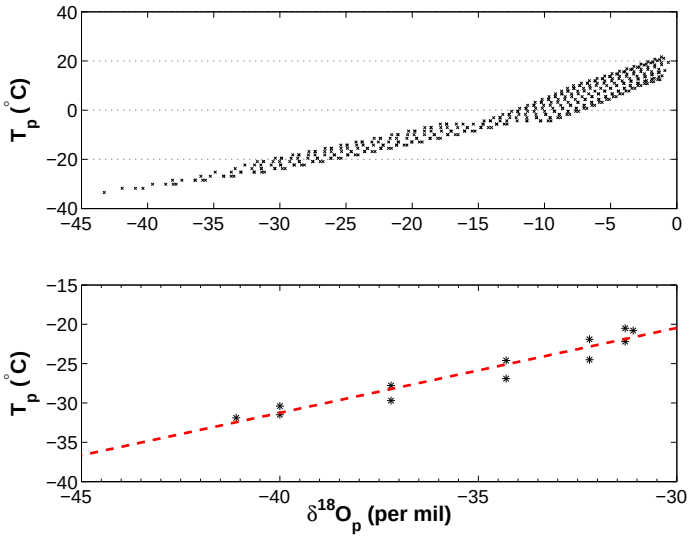

Figure 4.5: **Top**: T_p plotted against δ_p calculated with model II, using ship E as source. Results are for one annual cycle. Notice the kink in the data distribution around T_f. **Bottom**: Greenland site values for one annual cycle from same model run as above. The dashed line is the linear fit of the data points $T_p = (1.08 \pm 0.09)\delta^{18}O_p + (11.9 \pm 3.3)$.

Similar calculations have been done for Antarctica. Because of special meteorological conditions in Antarctica it is possible to compare model calculations with field measurements. In inland Antarctica there exists a strong

temperature inversion, making it possible to estimate the condensation temperature from the ground temperature. Jouzel & Merlivat [36] calculated the T_p-$\delta^{18}O_p$ relationship and also found it to be linear for for temperatures relevant for polar conditions. The calculated slope of 0.88°C/‰ (1.14‰/°C) was found to be very close to the experimental value.
From the T_p-$\delta^{18}O_p$ relationship found both for Greenland and Antartica, one must conclude that T_p and $\delta^{18}O_p$ is linearly related for low temperatures. Results from model I and II for Greenland show similar slopes, while the Antarctica slope is somewhat lower. It is not expected for the Greenland and Antarctic slopes to be the same, as the local meteorological conditions affect the slope. In Greenland the inversion layer is broken down by the passing of cyclonic systems, which transport the vapor. As model I and II are tuned for Greenland site values, tuning and trajectory differences is the most likely explanation for the differences obtained for the T_p–$\delta^{18}O_p$ slopes in Greenland and Antarctica.

4.2.3 Modeling the Deuterium Excess

As mentioned earlier the source for the Greenland moisture is matched by the ship E data. This match was found by simulating the monthly d_p for central Greenland, using Equation (4.1) to simulate the site $\delta^{18}O_p$. The annual d cycle of the ice cores shows a $\sim$ 3 month lag compared to the annual cycle of $\delta^{18}O$. This lag can only be reproduced using a lowlatitude source like ship E.
Figure 4.6 shows the monthly deuterium excess for Summit simulated by model II with ship E as source. The d_p seasonal cycle has a clear peak in September, while a broad undefined minimum appears from April to June. This is a reasonable simulation of timing of the excess cycle found in ice cores. The range of annual d_p values from about 5 to 13‰ also matches the data well (Johnsen et al. [35]).
The cause of the lag between the site d_p and $\delta^{18}O_p$ should be found in the site and source conditions. As already shown, $\delta^{18}O_p$ depends linearly upon T_p, so the $\delta^{18}O_p$ annual cycle is controlled by the T_p annual cycle at the site. The deciding factors for the site d_p is not as straight forward as for $\delta^{18}O_p$, but it will be shown that the most dominating parameter is the source temperature T_s. However, R_h and S_i also have an effect on d_p.
Figure 4.7 shows the effects of varying R_h with constant T_s (top plot), and the effects of varying T_s with constant R_h (bottom plot). In both cases the site d_p is affected by the variations in source conditions, but the impacts of varying R_h and T_s are different.

Increasing R_h decreases the site d_p. Higher relative humidity at the source thus results in lower excess at the site. The effect of increasing T_s is to decrease d_p. Thus, when the source temperature rises, the site excess rises. The fan-like shape of the plots in Figure 4.7 should also be noted. This shows that the effect on d_p of varying R_h decreases as the fractionation progresses, while the effect of T_s increases.
In Figure 4.7 R_h is varied from 0.5 to 1.0. The amplitude of the natural annual variation of R_h is not as strong. For ship E the monthly R_h ranges from 0.67 to 0.86. So in nature the effect of intra-annual variations of R_h on the site d_p cycle is limited. For T_s the variation from 15 to 25°C is close to the annual variations in a midlatitude source. The resulting range in d_p at the site of 10‰ is also close to the observed amplitude in ice cores from inland Greenland. So, the annual variation in T_s could account for the seasonal cycle in d_p.

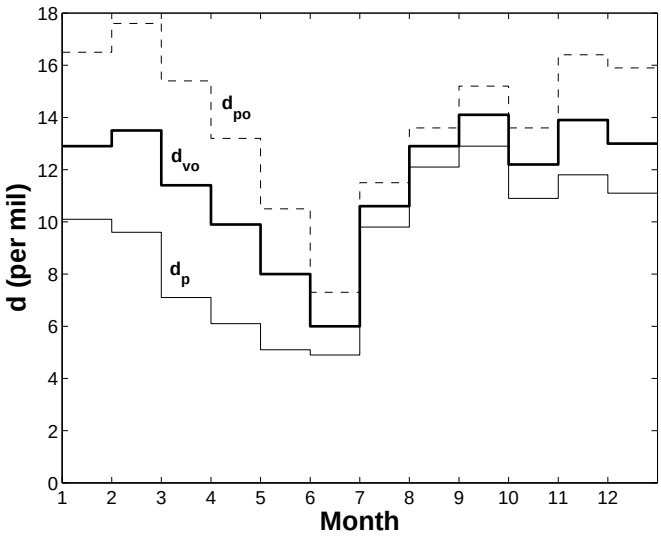

Figure 4.6: Monthly deuterium excess simulated by Model II for present day conditions with ship E as source, and using $S_i = 1.025 - 0.0033T$. The bold curve is the initial excess in the vapor at the source d_{vo}, the dashed curve is the excess in the first precipitation formed d_{po}, and the thin curve is the excess at Summit on the Greenland ice sheet d_p.

While observing the model behavior with different initial conditions it is noted, that d_p for the first condensate is almost constant, when only varying T_s, while great variations is seen in d_p when only varying R_h. When keeping R_h constant, then the kinetic effects during evaporation will also be constant,

so any differences in initial d_p will be caused by the temperature dependence of the equilibrium fractionation factor α. This can be verified by combining Equation (3.1) and (3.12)

$$\delta_{po} = \frac{\alpha_p}{\alpha_e} \frac{1-k}{1-kR_h} - 1 \tag{4.5}$$

where δ_{po} is the isotopic composition of the first condensate at dew point, α_p is the fractionation factor at the dew point, and α_e is the fractionation factor during evaporation. R_h is constant for all the model runs with different T_s, this means that for every run the parcel is cooled in approximately the same proportion before reaching dew point, which in turn means that the α_p/α_e relationship varies only little with T_s. As it turns out each parcel is fractionated to approximately the same degree just after reaching the dew point.

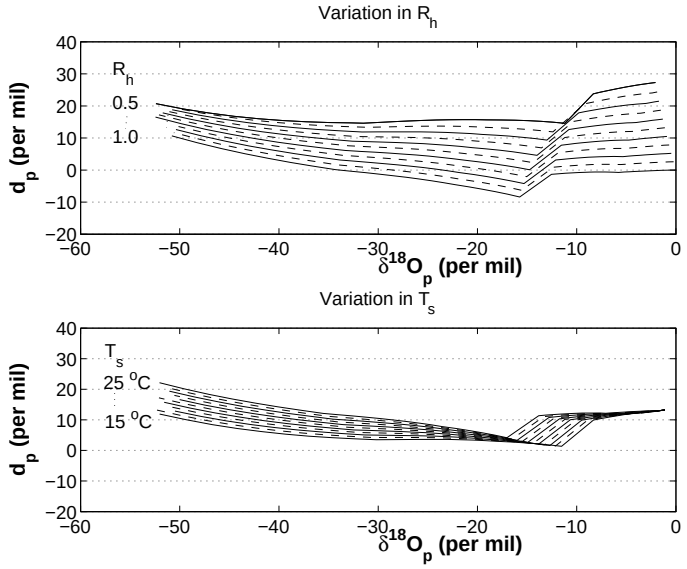

Figure 4.7: d_p plotted against $\delta^{18}O_p$ calculated with model II. **Top**: Variation in R_h from 0.5 to 1.0 in steps of 0.05 with a constant T_s of 20°C. **Bottom**: Variation in T_s from 15°C to 25°C in steps of 1°C with a constant R_h of 0.75.

When only varying either T_s or R_h the dew point is changed. As seen in Figure 4.7 the general slope of the curves changes when varying the source conditions. To keep the dew point constant R_h must be lowered while raising T_s. The result is shown in Figure 4.8.

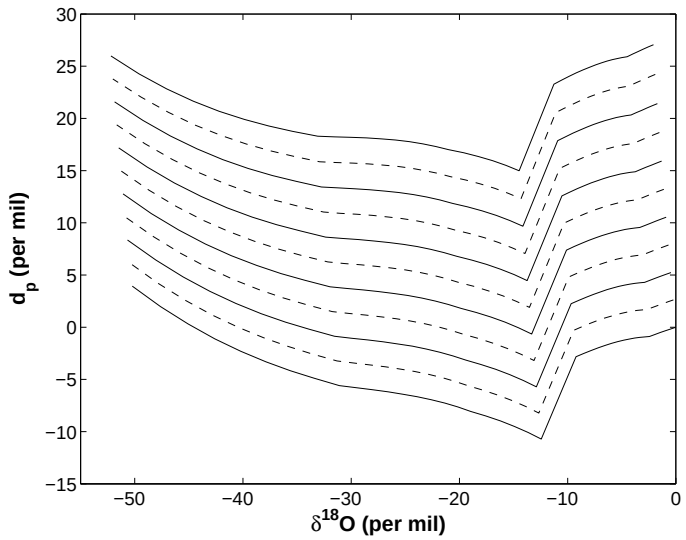

Figure 4.8: d_p plotted against $\delta^{18}O_p$ calculated with model II. The mixing ratio is held constant at $10g/kg$, while varying R_h from 0.5 to 1.0 in steps of 0.05 and T_s from 24.97°C to 14.01°C.

The curves for different source conditions are now approximately parallel. The conclusion to be drawn from this, is that the general $d - \delta^{18}O_p$ slope is controlled by the dew point.
The $d - \delta^{18}O_p$ slope is given by

$$\frac{\partial d}{\partial \delta^{18}O} = \frac{\partial(\delta D - 8\delta^{18}O)}{\partial \delta^{18}O} = \frac{\partial \delta D}{\partial \delta^{18}O} - 8 \tag{4.6}$$

so the $d_p - \delta^{18}O_p$ slope is essentially controlled by the $\delta D_p - \delta^{18}O_p$ slope, which can be found using Equation (3.5). Neglecting the $d\alpha/\alpha$ term in Equation (3.5), as it is almost one order of magnitude less than the dw_s/w_s term[1], the $\delta D_p - \delta^{18}O_p$ slope can be approximated by

$$\frac{\partial \delta D}{\partial \delta^{18}O} \cong \left(\frac{\delta D + 1}{\delta^{18}O + 1}\right)\left(\frac{\alpha_D - 1}{\alpha_{^{18}O} - 1}\right) \tag{4.7}$$

The dew point affects both of the fractions in parenthesis in Equation (4.7). The temperature dependence of α determines the size of the factors in the second parenthesis. A lower dew point will give a larger slope, as α_D increases more with temperature than $\alpha_{^{18}O}$. The first parenthesis is affected indirectly

[1] As stated by Jouzel & Merlivat [36].

by the dew point. A high dew point means that the condensation proces will have progressed further with respect to a given temperature compared to a situation with a low dew point. This means lower δ values in the high dew point situation. As δD decreases faster during condensation than $\delta^{18}O$, the slope will decrease with higher dew point. The effects of the first parenthesis will initially be small, as the δ values will be numerically small.
With the arguments above in mind, one can explain the behavior seen in Figure 4.7. Initally the $d_p - \delta^{18}O_p$ slope is positive and controlled by the temperature dependence of the fractionation factor. At T_f the fractionation factors changes because of kinetic effects affecting the slope. As the condensation progresses the slope decreases as a result of the $(\delta D + 1)/(\delta^{18}O + 1)$ relationship.

4.2.4 The Model Sensitivity with Respect to the Tuning of S_i

The S_i tuning greatly affects d_p, not only the annual mean value, but also the intra-annual variation. This is illustrated in Figure 4.9 which shows the annual cycle of d_p using two different S_i tunings. The bottom plot shows a very good correlation between d_p and T_s, which is less pronounced in the top plot. The bottom plot is produced using $F = 0.0041$ in the S_i parameterization. A larger value of F enhances the temperature dependence of the fractionation during deposition. As the annual cycle of the initial temperature still is partly intact in the early stages of deposition, some of the source temperature signal is preserved in d_p.
When using $F = 0.0033$ the temperature dependence is reduced, which causes the initial d_p signal controlled by R_h to be preserved. This is shown in Figure 4.10, where the annual site d_p cycle imitates the R_h cycle in the source region.
The effect that changes in S_i have on the site d_p has in this case little effect on the maximum and minimum d_p values during the year. It is the shape of the curve that changes also affecting the annual mean value.
Although the interpretation of the F tuning parameter seems correct, the annual cycle of d_p is affected by both C and F when tuning the model. Ultimately the tuning of S_i is a job of trial and error, where one only has few guide lines to follow.

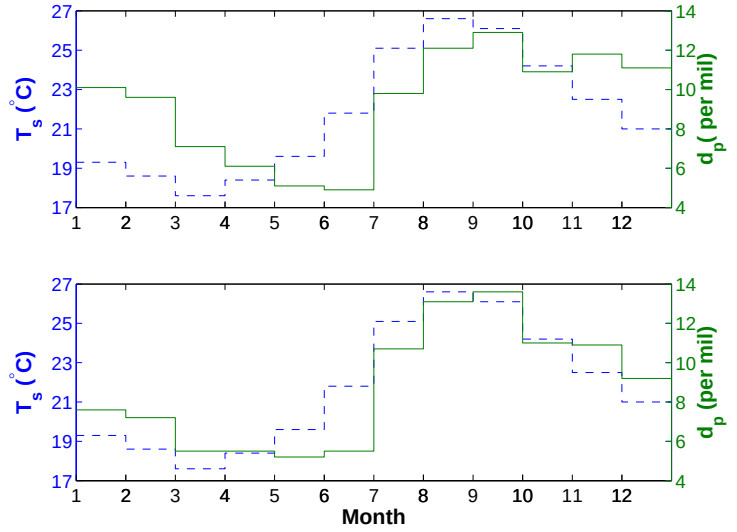

Figure 4.9: Monthly d_p (full line) from model II calculated with ship E as source plotted together with T_s (dashed). The top plot is produced with $S_i = 1.025 - 0.0033T$ and the bottom plot with $S_i = 1.03 - 0.0041T$.

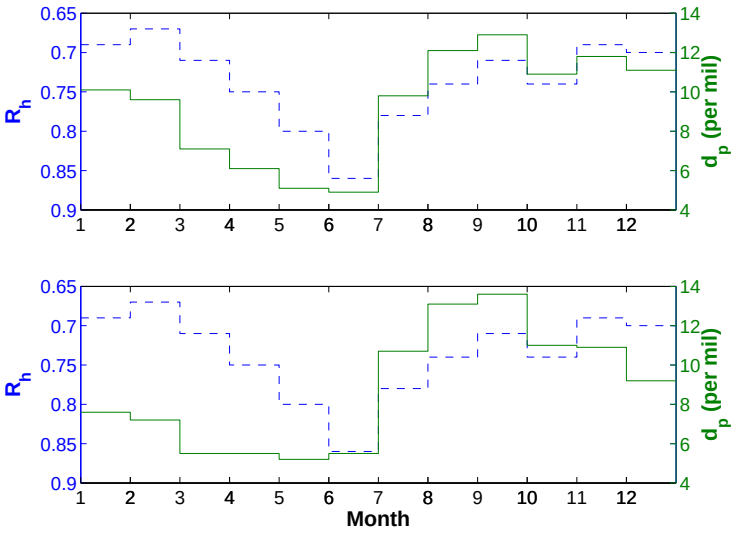

Figure 4.10: Monthly d_p (full line) from model II calculated with shipe E as source plotted together with R_h (dashed). The top plot is produced with $S_i = 1.025 - 0.0033T$ and the bottom plot with $S_i = 1.03 - 0.0041T$. Notice the R_h scale is reversed.

4.2.5 Discussion of Simple Isotopic Modeling

The simulation of δ values in precipitation using simple models with Rayleigh condensation involves many questionable assumptions. Examples are the highly idealized trajectory, source conditions described by a single set of parameters, complete glaciation of air parcel defined by T_f and the parameterization of the supersaturation.
To address the problem of the discontinuity at T_f, Ciais & Jouzel [11] have developed a Mixed Cloud Isotope Model (MCIM) which allows liquid water and ice crystals to coexist within a temperature interval. In this interval the MCIM simulates the Bergeron-Findeisen process (Section 2.4.3). This includes isotopic changes during evaporation of droplets and formation of ice crystals. The conclusion of Ciais & Jouzel, when comparing with earlier models, was that the simulation of the Bergeron-Findeisen process improves model results for the liquid-ice transition in the cloud, but for the polar site, models without the Bergeron-Findeisen process performs equally well.
The model used in this study does not include the Bergeron-Findeisen process, but the model results for Greenland should still be correct based on the findings of Ciais & Jouzel.
When dealing with the supersaturation during snow deposition, the simple models use a linear parameterization which is a function of temperature. The exact supersaturation is essentially unknown, so the model is tuned to the site conditions. The actual supersaturation is known to vary from one precipitation event to another and even within a single cloud. In the light of this S_i should be viewed as a mean supersaturation for the conditions along the trajectory above the North Atlantic and Greenland.
As discussed in Section 2.4.2 the supersaturation and snow formation is governed by micro physical processes, and requires knowledge of the dust composition in the air masses to be described. The S_i parameterization is a practical solution, that enables one to simulate δ values in precipitation with a minimum of data regarding local cloud conditions.
The performance of simple models have also been compared to more complex General Circulation Models (GCM), which included isotopic tracers in the water cycle. Such a comparison has been carried out by Armengaud et al. [1]. The conclusion was that the simple models largely reproduced the GCM results, when initialized with source conditions from the GCM. Some discrepancies between the two model types was also explained by inaccuracy in the GCM simulations.
The simple isotope models are an excellent tool for understanding the basic processes, that governs the δ values in the precipitation in the polar regions. However, the simplicity of the models limits the accuracy of the results. For

example are the trajectories and the parameterization of the supersaturation highly idealized. There is consequently a possibility that some parts of the models behavior may be artifacts.
Due to the nature of the simple isotope models, the uncercainty of the model results is hard to quantify. Therefore is the specific uncertainty of model results generaly not given in this study.

Chapter 5

Interpretation of the Greenland Ice Cores

This chapter is a presentation of the results obtained by the use of model II to interpretate Greenland ice core data. Additionally, recently published results are presented and discussed.

5.1 Recent Analysis and Modeling

To achieve a continuous temperature record for the GRIP site and source area Masson-Delmotte et al. [45] have proposed a method, which involves extracting T_{site} and T_{source} from the GRIP $\delta^{18}O$ and d. The method is based on the following equations obtained by multiple linear regression

$$\Delta T_{site} = 1.32\Delta\delta^{18}O_{corr} + 1.04\Delta d_{corr} \tag{5.1}$$

$$\Delta T_{source} = 0.29\Delta\delta^{18}O_{corr} + 1.58\Delta d_{corr} \tag{5.2}$$

where Δ is the anomalies from modern conditions, and the $corr$ suffix denotes that the $\delta^{18}O$ and d values have been corrected for any changes in the isotopic composition of the sea water. The numerical factors in Equation (5.1) and (5.2) are obtained by running the MCIM by Ciais & Jouzel [11] for various source conditions and then performing the multiple linear regression over a range of T_{site} and T_{source}.
The motivation of the model is that, if applying the modern spatial $\delta^{18}O$-temperature slope of $0.67‰/°C$ the glacial-interglacial temperature amplitude is underestimated by a factor of two when compared to results from borehole thermometry (results are discussed in Section 5.3). The solution

proposed, is to correct the $\delta^{18}O$ and d values for changes in annual precipitation distribution and intra-annual δ amplitude.
The present day seasonal distribution of precipitation for central Greenland is approximately equal in the summer and winter half of the year, with only a slightly larger amount of winter precipitation (Shuman et al. [59]). Past seasonality during the LGM has been estimated with GCM simulations showing an almost total lack of winter precipitation (Werner et al. [65]). The same simulation also showed an increased glacial $\delta^{18}O$ intra-annual amplitude (summer minus winter) of almost 30‰ compared to the present amplitude of 10‰ (Johnsen et al. [35]).
The change in seasonality across the glacial-interglacial transition results in a smaller shift in δ compared to a situation with no change in seasonality, caused by the lack of low winter δ values in the glacial period. A higher glacial intra-annual amplitude amplifies this effect because of less negative summer peaks.
Masson-Delmotte et al. [45] accounts for the changes in seasonality by introducing two thresholds. One is linked to the sea ice extent controlled by GRIP $\delta^{18}O$. When T_{site} derived from $\delta^{18}O$ is low enough, sea ice is assumed to inhibit the moisture supply. The other threshold is linked to the size of the Laurentide Ice Sheet (LIS), which is estimated from marine benthic $\delta^{18}O$. The increased size of LIS is assumed to shift winter storm tracks south ward, further inhibiting the winter moisture supply. Only when both threshold conditions are fulfilled is the seasonality taken into account. The seasonality correction is done using a simple summer-winter weighting. In this way the correction of the $\delta^{18}O$ and d values depends on the amount of summer precipitation and the intra-annual amplitude. The correction causes the $\delta^{18}O$-T_{site} slope to vary in time, resulting in a lower slope when the threshold conditions are fulfilled.
The approach described above results in an amplification of the D/O oscillations during the glacial and a larger transition amplitude in terms of temperature. The model results is in good agreement with temperature shifts achieved by other methods such as borehole thermometry (the transition) and gas fractionation (D/O oscillations) (Masson-Delmotte et al. [45]).

5.1.1 Discussion of Recent Isotope Modeling

From the values of the numerical factors in Equations (5.1) and (5.2) it is seen that T_{site} primarily is controlled by $\delta^{18}O$ and T_{source} is foremost controlled by d. This connection is parallel to the relationships found in this study shown in Section 4.2.1.

When producing Equation (5.1) and (5.2) only changes in T_{site} and T_{source} are taken into account. This means that important effects of changing R_h are neglected, which could be of importance when dealing with considerable changes of T_{source}.
In Equation (5.1) the factor of 1.32 relates $\delta^{18}O$ to T_{site}. This slope is close to the present day spatial slope of 0.67‰/°C as 1.32°C/‰ $\sim$ 0.75‰/°C. The slope of 0.75 is based on the output of the MCIM. However, the output of a simple isotope model like the MCIM only reflects conditions at the site during a precipitation event. The temperature during a precipitation event in central Greenland is different from the monthly mean temperature. During a precipitation event temperatures in central Greenland have been found to increase with as much as 20°C (Loewe [42]). In a temperature reconstruction it is the slope of $\delta^{18}O$ versus the mean site temperature, which is needed. This slope is unatainable with a simple isotope model.
As the site $\delta^{18}O$ mainly is a function of the cloud conditions[1] during a precipitation event the $\delta^{18}O$-T_{site} slope must depend on the number of precipitation events. A large difference between monthly mean temperature and the temperature during precipitation, as in the case of central Greenland, decreases the $\delta^{18}O$-T_{site} slope on a monthly basis.
Estimates of the temporal $\delta^{18}O$-T_{site} slope has been done with respect to different time scales. Shuman et al. [59] have calculated a slope on the basis of measured $\delta^{18}O$ from pit samples at the Greenland Summit versus a calculated surface temperature based on satellite measurements. This resulted in a slope of 0.46‰/°C for intra and inter-annual variations. For centennial variations Cuffey et al. [13] calculated a slope from borehole temperatures and $\delta^{18}O$ from ice core measurements. The result was a slope in the interval (0.45, 0.66)‰/°C.
These results for the temporal slope indicate that the temperature slope derived from the output of a simple isotope model, should not be used as the basis for extracting the mean temperature from ice core data. The simple models estimate a too large $\delta^{18}O$-T_{site} slope, because the precipitation temperature is significantly higher than the site mean temperature.
In the past few years it has become more common to use GCM's in the field of isotopic modeling. One example is the work done by Werner et al. [65], which has allready been mentioned. The quantitative quality of the results are however questionable. The model by Werner et al. is not able to convincingly simulate present day or LGM $\delta^{18}O$ values. This discrepancy is explained by the authors as being partly due to low model resolution. With a grid resolution of 3.75°×3.75° the GCM is not able to geometrically repre-

[1] See Section 4.2.1 for details.

sent cyclones, and thus correctly simulate the transport of water vapor to the high latitudes. With the lack of accuracy of the model in mind one should reconsider the seasonality and intra-annual amplitude of $\delta^{18}O$ adopted by Masson-Delmotte et al. [45].
A simple argument against the lack of winter precipitation found by Werner et al. [65] is based on the comparison of the $\delta^{18}O$ values in the GRIP and NGRIP ice cores (see Figure 5.1). The present day $\delta^{18}O$ values for GRIP and NGRIP are both close to -35‰ with the mean temperatures also being similar (NorthGRIP Members [49], and Johnsen et al. [34]). During LGM the NGRIP $\delta^{18}O$ is lower than the GRIP values. If central Greenland was lacking winter precipitation during LGM, one should expect this to be more pronounced when going north. This would cause the NGRIP $\delta^{18}O$ to be biased towards more positive values. As this is not the case significant winter precipitation did reach central Greenland during LGM.
The isotopic GCM simulations done by Jouzel et al. [37] are also worth mentioning, most notably the high resolution run. This run is a T42 resolution[2] simulation. Despite slightly better resolution than the model discussed above, there are still significant discrepancies compared to measured isotopic values. However, the model does produce some interesting results. The model produces a temporal $\delta^{18}O$-T_{site} slope that appears to be consistently lower than the spatial slope. This is in agreement with the estimated temporal slopes by Shuman et al. [59] and Cuffey et al. [13].
In spite of the problems presented here the approach of Masson-Delmotte et al. [45] still produce results that agree well with previous work. This of course supports the correctness of the temperature reconstruction. An objection to this argument is that, even if the method seem to reconstruct the temperature shifts, it is not guaranteed that the mechanisms behind are correct. As the method involves many uncertain parameters, like the seasonality, $\delta^{18}O$ amplitude, correction thresholds and MCIM parameters, it is possible to obtain a wide range of solutions. The point being that wrong mechanisms can lead to realistic results if the tuning permits it.
To summarize, the most important points of this discussion are listed below.

- The temporal and spatial $\delta^{18}O$-T_{site} slope are different, and are not interchangeable.
- The $\delta^{18}O$-T_{site} slope calculated with a simple isotope model cannot be applied directly to reconstruct T_{site} from ice cores.
- GCM simulations of isotopes are not reliable yet. Higher resolution is needed to accurately reproduce the measured data.

[2]The spectral resolution T42 corresponds to a 2.8°×2.8° grid resolution.

5.2 The Glacial General Circulation

The state of the atmospheric circulation is an indicator of climatic conditions. Variations of the past circulation can be extracted from ice core analysis. In this section recent results showing a modified glacial circulation are presented.

5.2.1 Glaciochemical Analysis as Circulation Proxy

The distribution of atmospheric aerosols depends on the general circulation of the atmosphere. Past changes in climate and circulation can thus be recovered from records of deposited material. The Greenland ice sheet is a source for such records, and the chemical composition of deep ice cores have been measured.

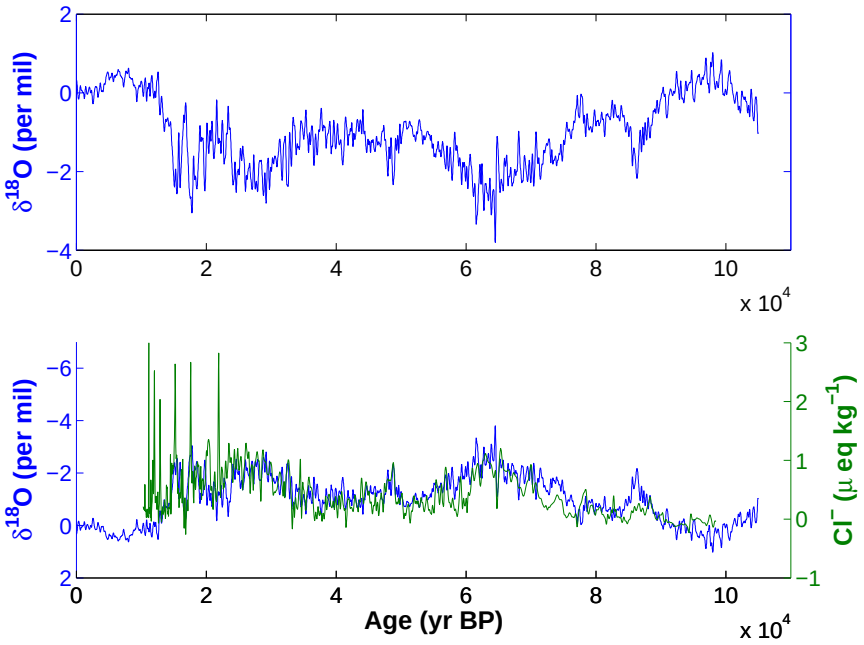

Figure 5.1: **Top**: $\delta^{18}O$ difference NGRIP-GRIP (NorthGRIP Members [49]). **Bottom**: NGRIP-GRIP $\delta^{18}O$ (blue) on a reversed scale plotted together with Cl^- concentration difference NGRIP-GISP2 (green) (Siggaard-Andersen [60]). All plots are on a common time scale. During the last part of the glacial and the early Holocene the Cl^- data is very noisy. This is partly due to contamination of the samples during measurements.

The atmospheric concentrations of different chemical species vary with the seasons. This variation reflects the conditions at the origin. Generally, the concentration of a species depends on the wind speed at its origin, with higher wind speeds resulting in higher concentrations (Genthon [22]). In this study the focus will be on two categories of species. One originating from sea salt and one from continental dust.
The dust found in Greenland ice cores originates from dust storms in the eastern Asian deserts. This dust is found as a spring-summer peak in the Greenland ice cores (Bory et al. [5]). In the case of sea salt the concentration peaks during the winter associated with higher wind speed over the oceans (Reader & McFarlane [55]). The concentrations of chemical species from dust and sea salt can thus be used as an indication of the seasonality of the Greenland precipitation, as aerosols arrive with the same air mass as the precipitation (Siggaard-Andersen [61]).
Regional differences in the chemical composition of ice cores can, with the arguments above in mind, reveal features of the past circulation. Figure 5.1 shows the NGRIP-GISP2 difference in Cl^- concentration reflecting the difference in deposited sea salt. The difference is plotted together with the NGRIP-GRIP difference[3] in $\delta^{18}O$ showing a striking resemblance between the two curves.
The similarity in the Cl^- and $\delta^{18}O$ differences can be explained by a circulation pattern involving two transport paths for moisture and aerosols to Greenland during the last glacial (Siggaard-Andersen [61]). One path from the south with a moisture source in the North Atlantic, and one north of LIS with a pacific moisture source. As NGRIP is located north of GRIP, NGRIP would receive more precipitation originating from the Pacific than GRIP due to inland moisture depletion of the air mass. Together with sea salt being a winter signal and the low NGRIP $\delta^{18}O$ values, the explanation is that during the winter NGRIP receives more moisture and sea salt from the Pacific than GRIP and GISP. This would result in the lower $\delta^{18}O$ values and higher Cl^- concentrations shown in Figure 5.1.
This glacial circulation pattern is supported by recent high resolution GCM mesoscale modeling done by Bromwich et al. [6]. This GCM has a 60km grid resolution, and is adapted for polar conditions. The boundary conditions are calculated by a global lower resolution GCM, and the major ice sheets are represented.
The simulated upper level circulation is shown in Figure 5.2. The areas of

[3]The GISP2 and GRIP sites are located geographically close, and are very similar in both chemical composition and isotope values. The GISP2 chemistry may be used instead of GRIP chemistry.

close isobars and high wind speeds define the mean placement of the jet stream, which is connected to high storm activity. Most importantly, the simulation shows a split jet stream in the winter period, with one branch south of LIS and one branch to the north. During the summer the northern branch weakens. The existence of a northern branch during the winter allows for cyclone to pass Greenland in a path from north west, transporting vapor originating from the Pacific.

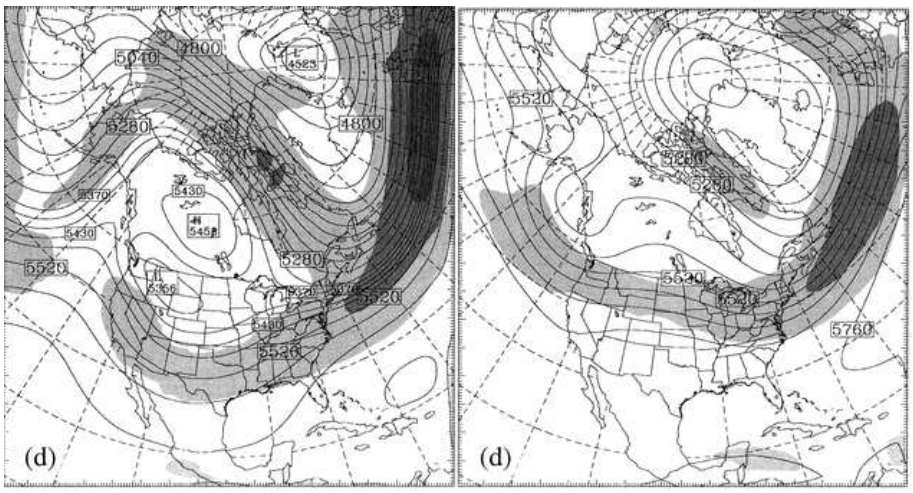

Figure 5.2: GCM simulation results for LGM showing the monthly mean 500hPa geopotential hight and wind speed for January (left) and July (right). Shaded areas are regions of high wind speed with the dark regions having the highest wind speed (adapted from Bromwich et al. [6]).

Bromwich et al. [6] have included a test of the sensitivity of the circulation with respect to the height of LIS. From this the conclusion is, that the main cause of the split jet stream is mechanical forcing by LIS on the atmosphere. The circulation pattern of additional moisture coming from northwest during the glacial, can also explain features of regional differences in other cores than GRIP, GISP2 and NGRIP. Two interesting cores are the Camp Century core from northwest Greenland, and the Renland core drilled in east Greenland near the coast (see map Figure A.2 in appendix).
The Camp Century core has a large glacial-interglacial $\delta^{18}O$ amplitude compared to the central Greenland ice cores. The Camp Century amplitude is around 12‰. This can be explained with the Camp Century site receiving a large amount of winter precipitation during the glacial. Because of the

Camp Century site location, storm tracks from northwest would probably be frequent during the winter if a split jet stream persisted. This would cause significant amounts of winter precipitation.
While the Camp Century core has a large glacial-interglacial $\delta^{18}O$ amplitude, the Renland core has an amplitude of only 4‰. The same line of arguments used to explain the Camp Century amplitude, can be applied to Renland only reversed. If the core lacks winter precipitation the glacial values would be high, resulting in a small amplitude. With the winter precipitation comming from the northwest, the location of the Renland site would inhibit winter precipitation. Air masses from the northwest would already have been depleted of moisture before reaching the Renland site, because of the shading effect of the ice sheet.

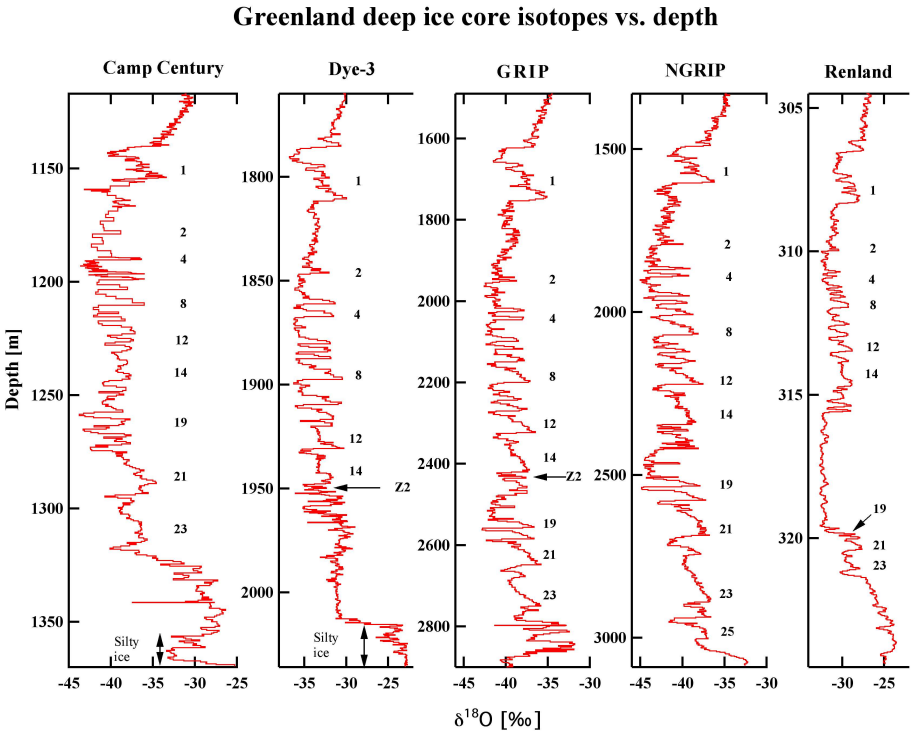

Figure 5.3: $\delta^{18}O$ values from five Greenland ice cores, all plotted on individual depth scales (Johnsen et al. [32]). Identifiable D/O oscillation are indicated.

In addition to the information from the $\delta^{18}O$ values from Camp Century and Renland, the chemical compositions have also been measured. The

Renland Cl^- show a low concentration with very little variation during the glacial. This further supports the idea of lack of winter precipitation at the Renland site (Siggaard-Andersen [60]).
Data of the chemical composition of the Camp Century core is very sparse. However, the existing data does show a larger Cl^- concentration compared to the Dye 3 core, drilled in the sounthern part of Greenland (Herron & Langway [26]). The points of this section are summarized below.

- The NGRIP-GISP2/GRIP difference in Cl^- concentration and $\delta^{18}O$ correlates.
- Split jet stream appears in high resolution GCM under LGM conditions.
- The glacial-interglacial $\delta^{18}O$ amplitude of Camp Century is large, and the Renland amplitude is small.
- The Renland core shows little variation in Cl^- concentration.

All of these points support the idea of a Pacific moisture source during the last glacial. This source supplied significant amounts of winter precipitation to central Greenland.

5.2.2 Variations in $\delta^{18}O$ and Deuterium Excess

The second order parameter, the deuterium excess (or simply the excess), is extensively being used to reflect changes in the circulation and the climate. Because of the excess dependence on source temperature, the state of the climate system can be investigated by comparing $\delta^{18}O$ and the excess.
In Figure 5.4 the variation in excess and $\delta^{18}O$ from the GRIP core is shown. The Figure shows an anticorrelation of the excess and $\delta^{18}O$ during the glacial on the time scale of thousands of years. The variations shown are D/O oscillations. With the low excess generally reflecting low source temperatures, it seems that the source is cold during the mild periods in Greenland. A similar anticorrelation has been shown for the Dye 3 ice core by Johnsen et al. [35].
The interpretation of the anticorrelation is that during the warm interstadials the sea ice retreats far to the north leaving open water. This could have given a larger contribution of moisture evaporated from higher latitudes with a lower T_{source} resulting in a lower excess.
As the sea ice retreats, the mean placement of the atmospheric polar front also moves further north. The polar front marks the onset of fractionation of precipitation, through development of cyclones. This means that the

fractionation process is less progressed when the cyclones reach Greenland, causing the precipitation to be less depleted in the interstadials compared to the stadials.

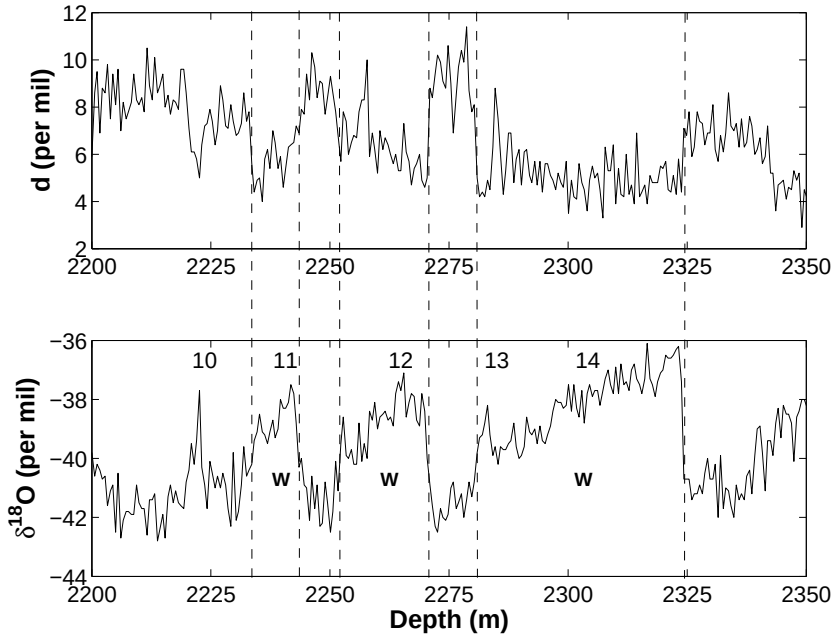

Figure 5.4: GRIP deuterium excess (top) and $\delta^{18}O$ (bottom) 55cm samples on a depth scale (Jouzel et al. [38]), with climate shifts marked by dashed lines. The most pronounced periods of high $\delta^{18}O$ are marked with W for warm, while numbers indicate identified interstadials. The section shown spans the period of about 38-50 kyr BP.

The anticorrelation of $\delta^{18}O$ and excess only appears during some periods of the last glacial. Figure 5.5 shows $\delta^{18}O$ and excess from the early part of the glaciation, when the large ice sheets were building up on the continents. This section of ice shows a positive correlation of $\delta^{18}O$ and excess, except for a periond of negative correlation in the section from 2650m to 2680m.
When the positive correlation is observed the temperature of the north Atlantic region must vary in phase showing the general climate trend of the region. The period of correlation shows that the climate system was still adjusting and had not yet entered full glacial mode.

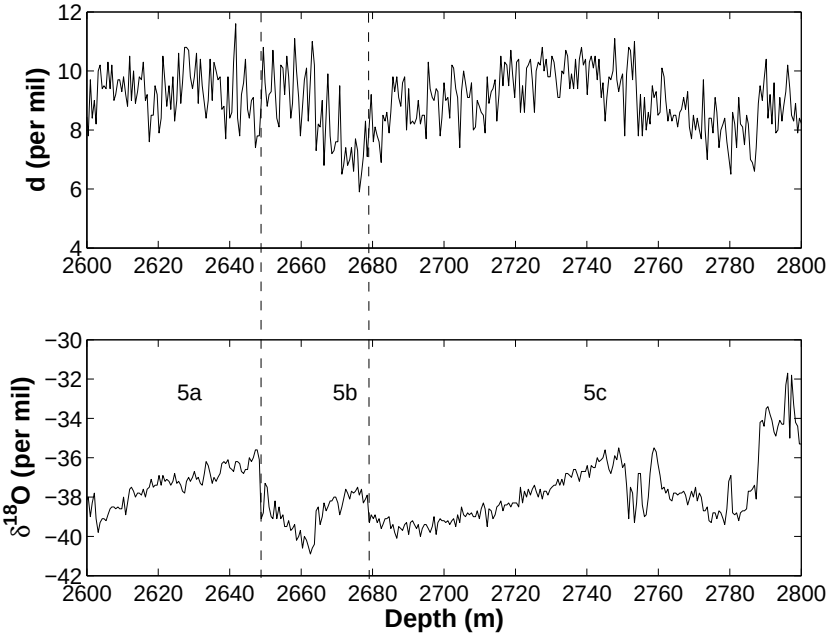

Figure 5.5: GRIP deuterium excess (top) and $\delta^{18}O$ (bottom) 55cm samples on depth scale (Jouzel et al. [38]). The numbering are the marine isotope stages. The section shown spans the period of about 80-105 kyr BP.

5.3 Modeling Glacial $\delta^{18}O$ and Deuterium Excess

To estimate temperature changes of the past 100 kyr using a simple isotope model a number of parameters must be set. As discussed in Section 5.1.1 problems arise, when trying to extract T_{site} directly from the measured $\delta^{18}O$ from ice cores, by the use of simple isotope modeling. The procedure in this study is therefore to use a temporal slope obtained from measurements and calculations done by Shuman et al. [59] and Cuffey et al. [13]. The results from these studies are not unanimous, but a good estimate of the $\delta^{18}O$-temperature slope would be $0.5‰/°C$. Compared to the use of the modern spatial slope, this gives a larger temperature change when extracting T_{site} from $\delta^{18}O$ during climate oscillations.
Seasonality can change the $\delta^{18}O$-temperature relationship if the ratio of the summer versus winter precipitation is altered. As other studies discussed earlier suggest, this can help to obtain the correct amplitudes of the temperatures extracted from climate oscillations seen in $\delta^{18}O$ (Masson-Delmotte et

al. [45]).
To experiment with the effect of seasonality a simple summer-winter weighting of the precipitation has been used when modeling. It is not obvious that the present approximately equal amounts of precipitation during the summer and winter should occur. As cold air can contain less moisture than warm air, then, for all else being equal, there should be more precipitation in the summer. However, presently an increased storm activity in the winter compensates for the lacking moisture in the cold air.
In a generally dryer glacial climate a bias towards more summer precipitation in the polar region is probable. Together with a higher glacial intra-annual $\delta^{18}O$ caused by a more vigorous jet stream, this alters the temperature interpretation. During the glacial the variabilily of the northern Atlantic ice extent and SST might have induced a greater intra-annual $\delta^{18}O$ amplitude. As shown in Figure 1.8 the marine polar front may have extended as far as 45-50°N during LGM. This also marks the boundary for the extent of winter sea ice (Ruddiman & McIntyre [56]). Recent results suggest that the North Atlantic was ice free as far north as Iceland (Meland et al. [46]). The consequence of this variability would have implications to the placements of the atmospheric polar front. With a larger meridional intra-annual movement of the polar front the $\delta^{18}O$ amplitude would increase. This is due to the fact, that the polar front is closely connected with the initiation of condensation and therefore also the fractionation of water molecules. This explanation is in favor of an increased glacial $\delta^{18}O$ amplitude. However, it does not present any quantitative estimate of the amplitude.
By using the $\delta^{18}O$-temperature slope of $0.5‰/°C$ a less dramatic seasonality correction is needed. A smaller seasonality correction is also compatible with the idea of an additional moisture source in the Pacific during the winter.
The effect of changing the seasonality can be investigated by using model II. The effect of changing the amount of winter precipitation from 50% to 28% is an increase in $\delta^{18}O$ of about 1.5‰. With an additional effect of increasing the intra-annual amplitude from the present 10‰ to 14‰, the seasonal correction amounts to approximately 2‰.
Apart from the seasonality correction the $\delta^{18}O$ values must be corrected for any changes in $\delta^{18}O$ in the sea water. The $\delta^{18}O_{sw}$ was higher during the glacial because of the depleted ice on the continents (Dansgaard & Tauber [17], Schrag et al. [58]). This means that the change in $\delta^{18}O_{sw}$ must be added to the $\delta^{18}O$ amplitude when considering changes from LGM to the present $\delta^{18}O$. A glacial-interglacial amplitude of 7‰ will then amount to 8‰, when correcting for the $\delta^{18}O_{sw}$ change.
The supersaturation during snow formation could also be different in a glacial environment. As discussed in Section 2.4 the formation of snow is affected

by the composition of dust aerosols. The different wind regime during the glacial may have affected the number, and size distribution of aerosols. This could have had an impact on rate of snow formation, and thus also the supersaturation. However, as the exact impact of any changes in the aerosols is unknown, the best option is to adopt the present day supersaturation parameterization found in this study to be $S_i = 1.025 - 0.0033T$.
All the ingredients needed to estimate temperature amplitude from LGM to present are now ready. With the glacial-interglacial amplitude of 7‰, seasonal correction of 2‰ and $\delta^{18}O_{sw}$ change of 1‰ , the corrected $\delta^{18}O$ amplitude adds up to 10‰. By using the $\delta^{18}O$-temperature slope of 0.5‰/°C the result is that central Greenland was 20°C colder during LGM.

	Present	LGM	Shift
$\delta^{18}O$ (‰)	-35	-42	7
d (‰)	9	6	3
T_{site} (°C)	-32	-52	20
T_{source} (°C)	22	17	5
	IST	ST	Shift
$\delta^{18}O$ (‰)	-37	-42	5
d (‰)	5	8	-3
T_{site} (°C)	-42	-52	10
T_{source} (°C)	18	20	-2

Table 5.1: Mean values of $\delta^{18}O$, d, T_{site} and T_{source} during different time periods for central Greenland. For Interstadials (IST) and stadials (ST) $\delta^{18}O$ and d are typical values. The shifts in T_{site} and T_{source} are estimated by the use of simple isotopic modeling. All numbers are given in round figures because of the uncertainty of the method.

Compared to independent estimates from borehole thermometry (Dahl-Jensen et al. [14]), which results in a temperature change of 23±2°C, the result presented here is of the right order of magnitude, but still underestimates the temperature change.
The $\delta^{18}O$ change of D/O oscillations is generally around 5‰. This results in a temperature change of 10°C, which is of the right magnitude compared to results from gas fractionation (Landais et al. [41]).
The source temperature during LGM can be estimated with model II. By simulating the LGM excess value of about 6‰, the mean T_{source} is found to be 17°C. This means that the LGM T_{source} was about 5°C colder than

present, as a consequence of the generally colder climate. In this calculation changes in R_h are not considered, as T_{source} is the most effective way of changing the site excess. Also, the knowledge of glacial values of R_h is very poor. A cooling of T_{source} by ~ 5°C is close to modeling results for LGM by Masson-Delmotte et al. [45].
As shown in Section 5.2.2 $\delta^{18}O$ and the excess generally anticorrelates during a D/O oscillation. The changes of the excess during the warming of Greenland is often around -3‰. When using model II the excess increases with decreasing $\delta^{18}O$ when the $\delta^{18}O$ values are low. This means that the excess will decrease with rising $\delta^{18}O$ even without changing T_{source}. Consequently, the excess decrease of 3‰ can be obtained with a cooling of T_{source} by 2°C. The model results are summarized in Table 5.1.
Two particular D/O oscillations are shown in Figure 5.6 in high temporal resolution to exemplify the abruptness of the climate shift. For both D/O 12 and 19 the shift happens in approximately 100 years. The shifts can be translated to a temperature change of 11°C and 14°C for D/O 12 and 19, respectively, using the slope of 0.5‰/°C. Although slightly underestimated, this is in the range of the temperatures obtained by gas fractionation of 12±3°C and 16±3°C for D/O 12 and 19, respectively (Landais et al. [41], [40]).

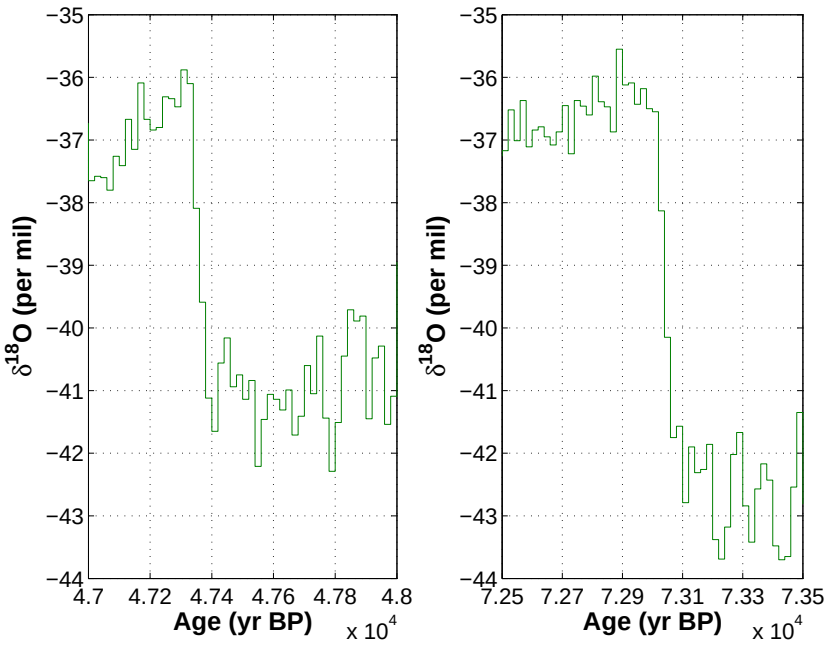

Figure 5.6: D/O oscillation 12 (left) and 19 (right) during the last glacial. Data is 20 yr averaged GRIP $\delta^{18}O$ (Johnsen et al. [32]).

The weakness of both LGM and D/O T_{site} and T_{source} reconstruction is, that model II is optimized to simulate scenarios with a single main moisture source area in the North Atlantic. With the possibillity of a Pacific winter moisture source, the interpretation of the isotopic values must be re-evaluated. There is of course the solution of the Pacific source being similar to the Atlantic, which would not alter the interpretation in terms of temperature. However, this would also depend on the history of the Pacific air mass.
The T_{site} amplitudes for both glacial-interglacial and D/O oscillations are generally slightly underestimated. As this seems to be systematic the explanation could be a wrong estimate of the general $\delta^{18}O$-temperature slope. The slope of $0.5‰/°C$ should perhaps be adjusted even lower, increasing the general amplitude of temperature variations extracted from isotope data. Another uncertainty factor in the temperature reconstruction is the seasonality correction. The magnitude of this correction is presently unknown.

Chapter 6

Summary and Outlook

Part of the work done in connection with this thesis, has been to modify the isotope model used by Johnsen et al. [35]. The modifications have been done to ensure, that the model was self-consistent with regard to the handling of micro physics connected with simulation of snow formation.
After the modification the model gives significantly different results. However, through tuning of model parameters it is possible to achieve similar results with the modified and original model. Ultimately, results presented by Johnsen et al. [35] using the original model are still valid, if one makes the assumption of a single Atlantic moisture source. This means that the present day main moisture source for central Greenland can be represented by data from Weathership E (35°N, 48°W). However, results are highly dependant on the parameterization of the supersaturation.
With the same assumption of a single Atlantic moisture source, the Last Glacial Maximum (LGM) source temperature has been simulated, using the modified model. The result is, that the LGM source temperature was ~ 5°C lower than the present source.
The possibility of using simple isotopic modeling to obtain a relationship between the mean Greenland site temperature and the site $\delta^{18}O$ has been investigated. The site $\delta^{18}O$ is highly dependent on the temperature in the cloud during a precipitation event. This means that the only information one can obtain from $\delta^{18}O$ measurements, is the temperature conditions during a precipitation event. Additional information on the local meteorogical conditions are nessasary to obtain the mean site temperature. In central Greenland the meteorogical conditions are too complex to extract the site temperature from simple isotope modeling. Further investigation of this subject is needed to quantify the mean temperature from $\delta^{18}O$.
To estimate the site temperature a $\delta^{18}O$-temperature slope from other studies is adopted (Shuman et al. [59], Cuffey et al. [13]). With this slope, and

corrections for seasonality and changes in $\delta^{18}O$ in sea water calculated with the isotope model, it is possible to calculate changes in the Greenland site temperature.
Results for the glacial-interglacial transition and selected Dansgaard-Oeschger oscillations obtained in this study are of the correct magnitude, but appear to be slightly underestimated compared to results achieved with other methods. This could be caused by the estimated $\delta^{18}O$-temperature slope or the seasonality correction.
Recent results discussed in Section 5.2, points to an additional main moisture source during the last glacial located in the Pacific. A Pacific moisture source during the last glacial can explain importent questions, that arise when comparing ice core data from different locations in Greenland. If the Pacific source in fact existed during the glacial the present interpretation of the $\delta^{18}O$ and deuterium excess should be re-evaluated.

Further simple isotopic modeling for Greenland could be done, involving a model modified to work with two main moisture sources. With this kind of model one could include a Pacific moisture source during the winter, and investigate the consequences for the deuterium excess and $\delta^{18}O$, using different ratios between sources.
With the recent development in isotopic GCM's further experimentation could provide invaluable information. GCM simulations with resolutions high enough to geometrically represent cyclones, would be able to simulate regional differences in the isotopic composition of the Greenland ice sheet, for both present and glacial conditions.
Simulations of the present conditions would give an impression of the models ability to recreate the currently observed isotopic composition. This would also give clues to the mechanisms controlling the temporal slope of $\delta^{18}O$ versus temperature. Glacial simulations would answer the question of the effect of a split jet stream caused by the presence of the Laurentide Ice Sheet.

Appendix A

A.1 The Vapor Pressure of Water

To calculate the water vapor pressure of air the Clausius-Clapeyron equation is used. The Clausius-Clapeyron equation arises by assuming equilibrium between the chemical potential of liquid water and water vapor[1], and is usually written as

$$\frac{de_s}{dT} = \frac{L}{T\Delta v} \tag{A.1}$$

where Δv is the difference between the volume of one molecule of water in the gas phase v_g and the volume of one molecule of water in the liquid phase v_l, e_s is the saturated vapor pressure of water, T is the temperature and L is the specific latent heat of evaporation. By assuming $v_g \gg v_l$ one may write

$$\Delta v \simeq v_g = \frac{V_g}{N_g}.$$

Using the ideal gas law $e_s V_g = N_g T$, we get

$$\Delta v \simeq T/e_s$$

The Clausius-Clapeyron Equation (A.1) can then be written as

$$\frac{de_s}{e_s} = \frac{LdT}{T^2}$$

We can now integrate the Clausius-Clapeyron equation by assuming the specific latent heat L is constant over our interval of integration.

$$\int_{e_{so}}^{e_s} \frac{de_s}{e_s} = L \int_{T_o}^{T} \frac{dT}{T^2}$$

[1] At least, this is done in the derivation by Kittel & Kroemer [39].

Resulting in a simple equation for the vapor pressure at a given temperature

$$e_s = e_{so} \exp\left(L\Big(\frac{1}{T_o} - \frac{1}{T}\Big)\right)$$

or expressed for one gram of vapor

$$e_s = e_{so} \exp\left(\frac{m_w L}{R}\Big(\frac{1}{T_o} - \frac{1}{T}\Big)\right) \tag{A.2}$$

By selecting e_{so} and T_o at the phase transition from solid to liquid, a useful equation for the water vapor content for meteorological purposes is obtained.

A.2 The Pseudoadiabatic Lapse Rate

A few definitions are necessary before commencing with the calculation of the pseudoadiabatic lapse rate.
The relationship between mixing ratio and vapor pressure is given by

$$w_s = \frac{\rho_w}{\rho_d} = \frac{R_d}{R_w}\frac{e_s}{p_d} = \epsilon\frac{e_s}{p - e_s} \simeq \epsilon\frac{e_s}{p}$$

where $p_d = p - e_s$ and $\epsilon = R_d/R_w$. w_s differentiates to

$$\frac{dw_s}{w_s} = \frac{de_s}{e_s} - \frac{dp}{p} \tag{A.3}$$

and de_s is calculated from equation (A.2)

$$de_s = e_s\frac{m_w L}{R}\frac{dT}{T^2}$$

The mixing ratio for the ambient air in the supersaturated regime w_a, is given by

$$w_a = w_s S_i$$

where S_i is the supersaturation with respect to ice saturation vapor pressure. Differentiating w_a gives

$$\frac{dw_a}{w_a} = \frac{de_s}{e_s} - \frac{dp}{p} + \frac{dS_i}{S_i} \tag{A.4}$$

The following is a deduction of the pseudoadiabatic lapse rate. The starting point is the first equation of thermodynamics

$$dq = du + pd\alpha$$

According to Joule u is alone a function of T for an ideal gas, that is

$$c_v = \frac{du}{dT}$$

so that

$$dq = c_v dT + pd\alpha$$

If one uses $d(p\alpha) = \alpha dp + pd\alpha$ one may write

$$dq = c_v dT + d(p\alpha) - \alpha dp$$

and then by use of the ideal gas law and $c_p \equiv c_v + R$ you get

$$dq = c_p dT - \alpha dp$$

The next step is to insert the heat of evaporation and hydrostatic balance. This is where the pseudoadiabatic assumption is made, as the only heat contribution during condensation considered in the system, is the heat from the condensating vapor $dq = -Ldw_s$. Any heat carried by liquid water is ignored assuming that all liquid is removed immediately after condensation.

$$-Ldw_s = c_p dT + gdz \tag{A.5}$$

and finally inserting dw_s from Equation (A.3) together with the ideal gas law and hydrostatic balance in the second term on the right, the equation now reads

$$c_p dT + gdz\left(1 + \frac{mLw_s}{RT}\right) + Lw_s \frac{de_s}{e_s} = 0$$

which in a few steps rewrites to the pseudoadiabatic lapse rate

$$\frac{dT}{dz} = -\frac{g}{c_p}\frac{\left(1 + \frac{mLw_s}{RT}\right)}{\left(1 + \frac{Lw_s}{c_p dT}\frac{de_s}{e_s}\right)}$$

In the supersaturated regime you get a similar result by inserting dw_a from (A.4) in Equation (A.5) instead of dw_s

$$\frac{dT}{dz} = -\frac{g}{c_p}\frac{\left(1 + \frac{mL_s w_s}{RT}\right)}{\left(1 + \frac{Lw_s}{c_p dT}\left(\frac{de_s}{e_s} + \frac{dS_i}{S_i}\right)\right)} \tag{A.6}$$

where L_s is the latent heat of sublimation.

A.3 Dynamic Meteorology

This section is a quick brush up on some of the equations and terms describing the dynamics of the circulation in the troposphere. Of special intrest is the mechanismes behind the polar jet stream and the development of synoptic disturbances. The equations and interpretations are from Holton [27] and vectors are given in bold.

A.3.1 The Thermal Wind Equation

The variation of the wind speed with height can be calculated from the hydrostatic equation and the geostrophic wind. The result is the thermal wind equation, here in isobaric coordinates

$$\frac{\partial \boldsymbol{V}_g}{\partial \ln p} = -\frac{R}{f}\boldsymbol{k} \times \boldsymbol{\nabla}_p T \tag{A.7}$$

where $\boldsymbol{V}_g$ is the geostrophic wind, p is pressure, R the gas constant, f the Coriolis parameter, $\boldsymbol{k}$ is the unit vector along the local vertical and T is the temperature. At a given latitude the wind will depend upon the temperature gradient. A temperature gradient will thus, according to Equation (A.7) give rise to a increasing wind with height which is perpendicular to the temperature gradient.
In a zone of large meridional temperature gradients such as the polar front, a upper level jet stream in the zonal direction will exist, because of the relationship described by Equation (A.7).

A.3.2 Vorticity

Cyclogenesis can be described with the theory of rotating fluids. One of the important terms in this matter is vorticity. The vorticity is defined as the curl of the velocity. In the case of motion on a rotating earth it is necessary to make a distinction between the absolute velocity and the relative velocity, writing the absolute velocity as

$$\boldsymbol{U}_a = \boldsymbol{U} + \boldsymbol{\Omega} \times \boldsymbol{r} \tag{A.8}$$

where $\boldsymbol{U}$ is the relative velocity, Ω is Earth's rotational vector and $\boldsymbol{r}$ is the distance to earths rotational axis. The last term on the right of Equation (A.8) is the velocity component due to Earth's rotation.

As the vorticity is defined as the curl of the velocity, we are now able to define the absolute and relative vorticity as

$$\boldsymbol{\omega}_a \equiv \boldsymbol{\nabla} \times \boldsymbol{U}_a, \qquad \boldsymbol{\omega} \equiv \boldsymbol{\nabla} \times \boldsymbol{U} \tag{A.9}$$

In general it is only the vertical components of Equation (A.9) that is of interest. These components are defined as

$$\eta \equiv \boldsymbol{k} \cdot (\boldsymbol{\nabla} \times \boldsymbol{U}_a), \qquad \zeta \equiv \boldsymbol{k} \cdot (\boldsymbol{\nabla} \times \boldsymbol{U}) \tag{A.10}$$

When considering the mechanismes of cyclogenesis it is the vertical component of the relative vorticity ζ, that should be considered. In the northern hemisphere cyclones form in regions of large positive ζ, while anticyclones is associated with negative ζ. Signs of ζ should be reversed when considering the southern hemisphere.
The sign of ζ and the upper level flow are linked in such a way, that the relationship between the upper level flow and surface pressure becomes as illustrated in Figure A.1. In general cyclones are thus formed to the east of a trough in the upper level pressure.

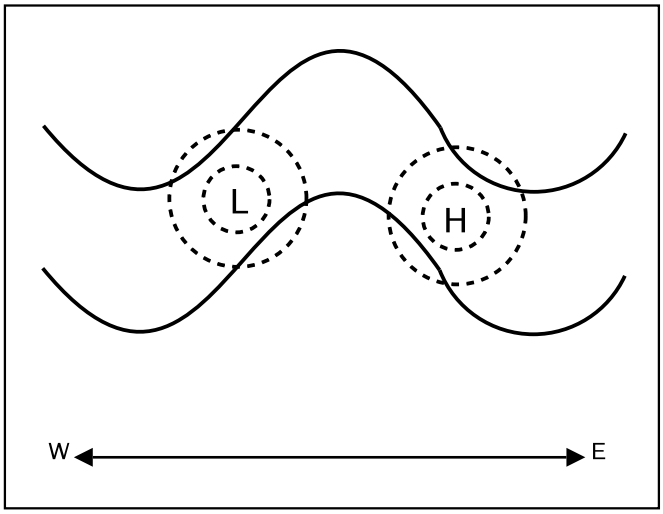

Figure A.1: Schematic view of the relationship between the upper level flow (solid) and the surface pressure (dashed). High and low surface pressure are marked by H and L, respectively.

A.4 Greenland Drill Sites

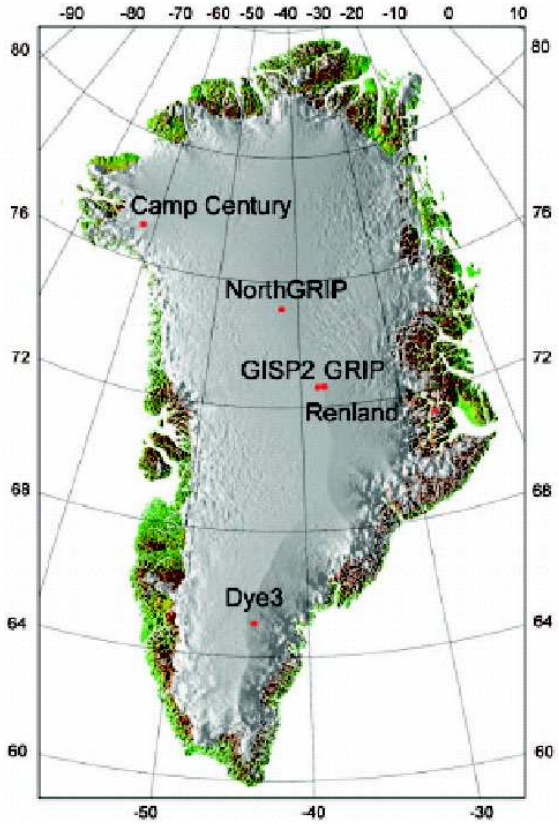

Figure A.2: The Greenland drill sites for deep ice cores marked on a map of the Greenland ice sheet.

Bibliography

[1] Armengaud, A., R.D. Koster, J. Jouzel, and P. Ciais. Deuterium excess in greenland snow: Analysis with simple and complex models. *J. Geophys. Res. 103* (1998), 8947–8953.

[2] Berger, A., and M.F. Loutre. Insolation values for the climate of the last 10 million years. *Quat. Sci. Rev. 10*, 4 (1991), 297–317.

[3] Bergeron, T. On the physics of cloud and precipitation. *Proc. 5th Assembly U.G.G.I. Lisbon 2* (1935).

[4] Bond, G., H. Heinrich, W. Broecker, L. Labeyrie, J. McManus, J. Andrews, S. Huon, R. Jantschik, S. Clasen, C. Simet, K. Tedesco, M. Klas, G. Bonani, and S. Ivy. Evidence for massive discharges of icebergs into the north atlantic ocean during the last glacial period. *Nature 360* (1992), 245–249.

[5] Bory, A.J.-M., P.E. Biscaye, A.M. Piotrowski, and J.P. Steffensen. Regional variability of ice core dust composition and provenance in greenland. *Geochem. Geophys. Geosys. 4*, 12 (2003).

[6] Bromwich, D.H., E.R. Toracinta, H. Wei, R.J. Oglesby, J.L. Fastook, and T.J. Hughes. Polar mm5 simulation of the winter climate of the laurentide ice sheet at the lgm. *J. of Climate 17* (2004), 3415–3433.

[7] Brutsaert, W. The roughness length for water vapor, sensible heat and other scalars. *J. Atmos. Sci. 32* (1975), 2028–2031.

[8] Brutsaert, W.A. Theory for local evaporation (or heat transfer) from rough and smooth surfaces at ground level. *Water Resour. Res. 11* (1975), 543–550.

[9] Byers, H. *Elements of Cloud Physics.* The University of Chicago Press, 1965.

[10] Cappa, C.D., M.B. Hendricks, D.J. De Paolo, and R.C. Cohen. Isotopic fractionation of water during evaporation. *J. Geophys. Res. 108* (2003), 4525–4534.

[11] Ciais, P., and J. Jouzel. Deuterium and oxygen 18 in precipitation: Isotopic model, including mixed cloud processes. *J. Geophys. Res. 99* (1994), 16793–16803.

[12] Craig, H. Isotopic variations in meteoric waters. *Science 133* (1961), 1702–1703.

[13] Cuffey K.M., R.B. Alley, P.M. Grootes, J.M. Bolzan, and S. Anandakrishnan. Calibration of the $\delta^{18}o$ isotopic paleothermometer for cantral greenland, using borehole temperatures. *J. of Glaciology 40* (1994), 341–349.

[14] Dahl-Jensen, D., K. Mosegaard, N. Gundestrup, G.C. Clow, S.J. Johnsen, A.W. Hansen, and N. Balling. past temperatures direcly from the greenland ice sheet. *sc 282* (1998), 268–271.

[15] Dansgaard, W. Stable isotopes in precipitation. *Tellus 16* (1964), 436–468.

[16] Dansgaard, W. The abundance of o^{18} in atmospheric water and water vapor. *Tellus 5* (1953), 461–469.

[17] Dansgaard, W., and H. Tauber. Glaicier oxygen-18 content and pleistocene ocean temperatures. *Science 166* (1969), 499–502.

[18] Dansgaard, W., S.J. Johnsen, H.B. Clausen, D. Dahl-Jensen, N.S. Gundestrup, C.U. Hammer, C.S. Hvidberg, J.P. Steffensen, A.E. Sveinbjàrnsdottir, J. Jouzel, and G. Bond. Evidence for general instability of past climate from a 250-kyr ice-core record. *Nature 364* (1993), 218–220.

[19] Epstein, S., and T. Mayeda. Variations of the o^{18} content of waters from natural sources. *Geochem. et Cosmochim. Acta 4* (1953), 213–224.

[20] Findeisen, W. Die kolloidmeteorologischen vorgänge bei der niederschlagsbildung (colloid meteorological processes in the formation of precipitation). *Met. Z. 56* (1938).

[21] Fuchs, A., M.C. Leuenberger. Delta o-18 of atmospheric oxygen measured on the grip ice core document stratigraphic disturbances in the lowest 10% of the core. *Geophys. Res. Lett. 23* (1996), 1049–1052.

[22] GENTHON, C. Simulations of the long range transport of desert dust and sea-salt in a general circulation model. In *Precipitation scavenging and atmosphere-surface exchance*, vol. 3. Hemisphere publishing corporation, 1992, pp. 1783–1794.

[23] HADLEY, G. Concerning the cause of the general trade winds. *Phil. Trans. R. Soc. 39* (1735), 58–62.

[24] HAMMER, C.U., H.B. CLAUSEN, W. DANSGAARD, A. NEFTEL, P. KRISTINSDOTTIER, AND E. JOHNSEN. Continuous impurity analysis along the dye 3 deep core. *Geophysical Monograph 33* (1985).

[25] HAYS, J.D., J. IMBRIE, AND N.J. SHACKLETON. Variations in the earth's orbit: Pacemaker of the ice ages. *Science 194* (1976), 1121–1132.

[26] HERRON, M.M., AND C.C. LANGWAY. Chloride, nitrate, and sulfate in the dye 3 and camp century ice cores. *Geophysical Monograph 33* (1985).

[27] HOLTON, J. *An Introduction to Dynamic Meteorology*, third ed. Academic Press, 1992.

[28] IAEA/WMO. Inetrnational Atomic Energy Agency/World Meteorological Organization, 1969-79. *Envirinmental isotope data No. 1-6.* World survey of isotope concentration in precipitation. *Technical reperts series*, Nos. 96, 117, 129, 147, 165 and 192. *I.A.E.A., Vienna.*

[29] IMBRIE, J., AND A. DUFFY ET AL. Specmap archive # 1. *IGBP PAGES/World Data Center-A for Paleoclimatology Data Contribution Series # 90-001. NOAA/NGDC Paleoclimatology Program, Boulder CO, USA* (1990).

[30] JOHNSEN, S.J. Stable isotope homogenization of polar firn and ice. *Proceedings of a symposium held during the XVI Assembly of the International Union of Geodesy and Geophysics at Grenoble, August/September 1975; Actes du colloque de Grenoble, Août/Septembre 1975 IAHS-AISH Publ. No. 118* (1977), 210–219.

[31] JOHNSEN, S.J, AND W. DANSGAARD. On flow model dating of stable isotope records from greenland ice cores. In *The Last Deglaciation: Absolute and Radiocarbon Chronologies*, vol. I 2 of *Nato ASI.* Springer-Verlag Berlin Heidelberg, 1992, pp. 13–24.

[32] Johnsen, S.J., D. Dahl-Jensen, N. Gundestrup, J.P. Steffensen, H.B. Clausen, H. Miller, V. Masson-Delmotte, A.E. Sveinbjàrndottir, and J. White. Oxygen isotope and palaeotemperature records from six greenland ice-core stations: Camp century, dye-3, grip, gisp2, renland and northgrip. *J. Quat. Sci. 16* (2001), 299–307.

[33] Johnsen, S.J, D. Dahl-Jensen, W. Dansgaard, and N. Gundestrup. Greenland palaeotemperatures derived from grip bore hole temperature and ice core isotope profiles. *Tellus 47B* (1995), 624–629.

[34] Johnsen, S.J., H.B. Clausen, W. Dansgaaed, F. Fuhrer, N. Gundestrup, C.U. Hammer, P. Iversen, J. Jouzel, B. Stauffer, and J.P. Steffensen. Irregular glacial interstadials recorded in a new greenland ice core. *Nature 359* (1992).

[35] Johnsen, S.J, W. Dansgaard, and J.W.C. White. The origin of arctic precipitation under present and glacial conditions. *Tellus 41B* (1989), 452–468.

[36] Jouzel, J., and L. Merlivat. deuterium and oxygen 18 in precipitation: Modeling of the isotopic effects during snow formation. *J. Geophys. Res. 89* (1984), 11749–11757.

[37] Jouzel, J., G. Hoffmann, R.D. Koster, V. Masson. Water isotopes in precipitation: data/model comparison for present-day and past climates. *Quat. Sci. Rev. 19* (2000), 363–379.

[38] Jouzel, J., V. Masson-Delmotte, M. Stievenard, A. Landais, F. Vimeux, S.J. Johnsen, A. Sveinbjàrndottir, and J.W.C. White. Rapid deuterium-excess changes in greenland ice cores: a link between the ocean and the atmosphere. *In preparation.*

[39] Kittel, C., and H. Kroemer. *Thermal Physics*, second ed. W.H. Freeman and Company, 2000.

[40] Landais, A., J.M. Barnola, V. Masson-Delmotte, J. Jouzel, J. Chappellaz, and N. Caillon. A continuous record of temperature evolution over a sequence of dansgaard-oeschger events during marine isotopic stage 4 (76 ti 62 kyr bp). *Geophys. Res. Lett. 31* (2004).

[41] Landais, A., N. Caillon, C. Goujon, A.M. Grachev, J.M. Barnola, J. Chappellaz, J. Jouzel, V. Masson-Delmotte and M. Leuenberger. Quantification of rapid temperature change during

do event 12 and phasing with methane inferred from air isotopic measurements. *Earth and Plan. Sc. Lett. 225* (2004), 221–232.

[42] LOEWE, F. The greenland ice cap as seen by a meteorologist. *Quart. Journ. Roy. Meteorol. Soc. 62* (1936), 359–377.

[43] MAJOUBE, M. Oxygen-18 and deuterium fractionation between water and steam. *J. Chim. Phys. 10* (1971).

[44] MASON, B. *The Physics of Clouds*, second ed. Oxford University Press, 1971.

[45] MASSON-DELMOTTE, V., J. JOUZEL, A. LANDAIS, M. STIVENARD, S.J. JOHNSEN, J.W.C. WHITE, M. MERNER, A. SVEINBJÀRNDOTTIR, AND K. FUHRER. Grip deuterium excess reveals rapid and orbital-scale changes in greenland moisture origin. *Science 309* (2005).

[46] MELAND, M.Y., E. JANSEN, AND H. ELDERFIELD. Constraints on sst estimates for the northern north atlantic/nordic seas during the lgm. *Quat. Sci. Rev. 24* (2005), 835–852.

[47] MERLIVAT, L. Molecular diffusivities of $H_2^{16}O$, $HD^{16}O$, and $H_2^{18}O$ in gases. *J. Chem. Phys. 69* (1978), 2864–2871.

[48] MERLIVAT, L., AND J. JOUZEL. Global climate interpretation of the deuterium-oxygen 18 relationship. *J. Geophys. Res. 84* (1979), 5029–5033.

[49] NORTH GREENLAND ICE-CORE PROJECT (NORTHGRIP) MEMBERS. High resolution climate record of the northern hemisphere back into the last interglacial period. *Nature 431* (2004), 147–151.

[50] PELTIER, W.R. On eustatic sea level history: Last glacial maximum to holocene. *Quat. Sci. Rev. 21* (2002), 377–396.

[51] PERRY, A.H., AND J.M. WALKER. *The ocean-atmosphere system.* Longman Inc., 1977.

[52] RAHMSTORF, S. Ocean circulation and climate during the past 120,000 years. *Nature 419* (2002), 207–214.

[53] RASMUSSEN, S.O., K.K. ANDERSEN, A.M. SVENSSON, J.P. STEFFENSEN, B.M. VINTHER, S.J. JOHNSEN, H.B. CLAUSEN, L.B.

Larsen, M. Bigler, R. Röthlisberger M.-L. Siggaard-Andersen, H. Fischer, U. Ruth, K. Goto-Azuma, and M. Hanson. A new greenland ice core chronology for the last galcial termination. *In preparation.*

[54] Rasmussen, S.O., K.K. Andersen, M.-L. Siggaard-Andersen, and H.B. Clausen. Extracting the annual signal from greenland ice-core chemistry and isotopic records. *Annals of Glaciology 35* (2002), 131–135.

[55] Reader, M.C., and N. McFarlane. Sea-salt aerosol distribution during the last glacial maximum and its implications for mineral dust. *J. Geophys. Res. 108* (2003).

[56] Ruddiman, W.F., and A. McIntyre. The north atlantic ocean during the last deglaciation. *Palaeogeogr., Palaeoclimatol., Palaeocol. 35* (1981), 145–214.

[57] Salby, M.L. *Atmospheric Physics.* Academic Press, 1996.

[58] Schrag, D.P., J.F. Adkins, K. McIntyre, J.A. Alexander, D.A. Hodell, C.D. Charles, and J.F. McManus. The ocean oxygen isotopic composition of the seawater during the last glacial maximum. *Quat. Sci. Rev. 21* (2002), 331–342.

[59] Shuman, C.A., R.B. Alley, S. Anandakrishnan, J.W.C. White, P.M. Grootes, and C.R. Stearns. Temperature and accumulation at the greenland summit: Comparison of high-resolution isotope profiles and satellite passive microwave brightness temperature trends. *J. Geophys. Res. 100* (1995), 9165–9177.

[60] Siggaard-Andersen, M.-L. A continuous ic glaciochemical record of the last glacial period from the ngrip ice core. *In preparation.*

[61] Siggaard-Andersen, M.-L. *Analysis of soluble ions from dust and sea salt over the last glacial cycle in polar deep ice cores.* PhD thesis, Alfred Wegener Institute für Polar -und Meeresforschung, Fachbereich Geosystem, Columbus Strasse, 27568 Bremerhaven, Germany, 2005.

[62] Strickley, A.R. An evaluation of the bergeron-findeisen precipitatiuon theory. *Monthly Weather Review 69* (October 1940), 272–280.

[63] Vali, G. Ice nucleation-theory – a tutorial. http://www-das.uwyo.edu/∼vali, 1999.

[64] WEGENER, A. *Thermodynamik der atmosphäre.* Barth, Leipzig, 1911.

[65] WERNER, M., U. MIKOLAJEWICS, M. HEIMANN, AND G. HOFFMANN. Borehole versus isotope temperatures on greenland: Seasonality does matter. *Geophys. Res. Lett. 27* (2000), 723–726.

[66] ZWECK, C., AND P. HUYBRECHTS. Modeling of the northern hemisphere ice sheets during the last glacial cycle and glaciological sensitivity. *J. Geophys. Res. 110* (2005).